



**Photocatalytic degradation of orange II sodium dye in textile wastewater
using TiO₂-supported with activated carbon**

By

MUSUNGAY TSHIBOLA LAURY

Dissertation submitted in fulfilment of the requirements for the

Degree

Master of Applied Science: Chemistry

in the

Faculty of Applied Sciences

at the

Cape Peninsula University of Technology

Supervisor: Dr Francois Wewers

Co-Supervisor: Dr Kassim Badmus

Bellville

January 2022

CPUT copyright information

The dissertation/thesis may not be published either in part (in scholarly, scientific or technical journals), or as a whole (as a monograph), unless permission has been obtained from the University

DECLARATION

I, **MUSUNGAY TSHIBOLA LAURY**, declare that the contents of this dissertation/thesis represent my own unaided work and that the dissertation/thesis has not previously been submitted for academic examination towards any qualification. Furthermore, it represents my own opinions and not necessarily those of the Cape Peninsula University of Technology.

Signed

Date

ABSTRACT

Azo dyes are the most used dyes in the textile industry. Azo dyes are also the most harmful in the environment due to their soaring toxicity, and bio-recalcitrance for common microbial wastewater treatment. Photocatalytic degradation using titanium dioxide (TiO_2) has been found effective in their treatment in wastewater. However, the large energy band gap of TiO_2 (2.80 - 3.20 eV) makes TiO_2 absorb less than 5 % in the visible spectrum. Supporting TiO_2 with a non-metal can enhance the photocatalytic activity of TiO_2 and allow the use of a larger amount of solar energy. A non-metal such as carbon is mostly used as photocatalyst support due to its stability, mechanical resistance, and elevated superficial area.

In this study, the photocatalytic degradation process of orange II sodium dye was investigated by using TiO_2 -supported biochar nanoparticles as photocatalyst. TiO_2 -supported biochar composites were synthesised by an ultrasound process by mixing TiO_2 and biochar using the ratio 3:2 (60% biochar and 40% TiO_2). TiO_2 was synthesized from TiCl_3 via a hydrothermal process and biochar was obtained by carbonization of *Acacia saligna* (Port Jackson Willow) leaves. Biochar, TiO_2 and TiO_2 -supported biochar nanoparticles were characterised by UV-Vis spectrophotometry, Scanning Electron Microscopy-Energy Dispersive Spectroscopy (SEM-EDS), Fourier transformer infrared (FTIR), X-ray diffraction (XRD), and Brunauer-Emmett-Teller (BET). Compared with the synthesised TiO_2 (band gap = 2.81 eV), the energy band gap of TiO_2 -supported biochar composite was measured to be 2.11 eV, showing comparatively more promise as a solar active photocatalyst. Results from FTIR and SEM-EDS confirmed that TiO_2 was successfully immobilized on the biochar external surface. The BET results showed curves of TiO_2 and TiO_2 supported biochar composites exhibiting small hysteresis phenomena which represent a typical type-IV isotherm attributed to mesoporous material with low porosity. Furthermore, the XRD results revealed the presence of rutile and anatase crystalline phases in the TiO_2 -supported biochar composites, due to the doping of biochar.

The photocatalytic activity of TiO_2 and TiO_2 -supported biochar composites were studied for the removal of orange II sodium dye. Batch experiments were conducted to obtain the optimum conditions for the dye degradation. The effect of parameters such as pH, photocatalyst loading and initial dye concentration was determined. From the results obtained in this study, the optimum

conditions obtained were 120 min contact time for both nanoparticles using 200 mg/L for TiO₂-supported biochar at pH 6.8 and TiO₂ at pH 4, respectively. The highest degradation efficiency of orange II sodium was found to be 20.75 % using TiO₂ at pH 4 and 83.48 % using TiO₂-supported biochar at pH 6.8. The photocatalytic degradation of orange II sodium followed the pseudo-first-order kinetic ($r^2 = 0.9914$) with the lowest EE_o of 136.49 kWh/m³ using TiO₂-supported biochar at pH 6.8; thus, reducing the process' cost. TiO₂-supported biochar composites were found to be effective in the photocatalytic degradation of orange II sodium dye in a neutral solution. In addition, TiO₂-supported biochar composites showed good stability without any significant loss over three reusability cycles.

ACKNOWLEDGEMENTS

First of all, I am grateful to the Almighty God for giving me strength, knowledge, ability and opportunity to undertake this research study and to persevere and complete it despite the difficult times. Without His blessings, this achievement would not have been possible.

A profound sense of gratitude to my supervisor Dr Francios Wewers who made this thesis possible by his valuable guidance, encouragement and support.

I wish to express my sincere gratitude to Dr Kassim Badmus, for his help and understanding which make this thesis possible.

I am also thankful to Department of chemistry in applied science and all the laboratory staff for helping with equipment and other essential services in the laboratory.

No words of thanks to my mother Claudine Tshituka Tshendele, all I am or ever hope to be, I owe it to you. You are my rock.

I would like to give thanks to my sister Justine and Brothers Marco, Adam, Gloris and Ryan. Without their endless encouragement, love, and support, completing this thesis would have been impossible. I am deeply grateful to them for each day of my life and my expression of thanks is not enough.

My thanks and appreciation also go to my friends and laboratory colleagues.

DEDICATION

In loving memory of a special Dad

KANKU MUSUNGAYI BENOIT

Always on my mind. Forever in my heart.

TABLE OF CONTENTS

DECLARATION.....	i
ABSTRACT	ii
ACKNOWLEDGEMENTS	iv
DEDICATION	v
TABLE OF CONTENTS	vi
LIST OF TABLES	ix
LIST OF FIGURES.....	x
LIST OF ABBREVIATIONS AND SYMBOLS.....	xii
CHAPTER 1.....	1
INTRODUCTION.....	1
1.1. BACKGROUND	1
1.2. PROBLEM STATEMENT.....	2
1.3. AIM AND OBJECTIVES	3
1.4. RESEARCH QUESTIONS	3
1.5. SIGNIFICANCE OF THE RESEARCH.....	4
1.6. DELINEATION	4
1.7. RESEARCH ASSUMPTIONS.....	4
CHAPTER 2.....	5
LITERATURE REVIEW.....	5
2.1. CHARACTERISTICS OF TEXTILES WASTEWATER	5
2.2. TEXTILE DYES	5
2.3. CONVENTIONAL TREATMENT OF AZO DYES IN TEXTILE WASTEWATER ..	7
2.3.1. Primary treatment	7
2.3.2. Secondary treatment	7
2.3.3. Tertiary treatment	8
2.4. ADVANCED OXIDATIVE PROCESSES (AOPs).....	8
2.5. HETEROGENOUS PHOTOCATALYSIS	10
2.6. TiO ₂ MODIFICATIONS	11
2.6.1. Non-metal doping.....	12
2.6.2. Metal oxide doping.....	13
2.6.3. Metal-ion doping	13
2.7. PORT JACKSON WILLOW (<i>ACACIA SALIGNA</i>).....	14
2.7.1. Identification of the Port Jackson Willow	14

2.7.2.	Invasion of the Port Jackson Willow in South Africa	14
2.8.	SYNTHESIS OF BIOCHAR (CARBON)	15
2.9.	SYNTHESIS OF TiO ₂ -SUPPORTED BIOCHAR COMPOSITES	16
2.9.1.	Sol-gel process	16
2.9.2.	Solvothermal process	16
2.9.3.	Sonochemical process	17
2.10.	TiO ₂ -SUPPORTED CARBON COMPOSITES IN PHOTOCATALYSIS	17
CHAPTER 3	21
METHODOLOGY	21
3.1.	CHEMICAL REAGENTS AND MATERIALS	21
3.2.	PREPARATION OF PHOTOCATALYST NANOCOMPOSITES AND SIMULATED TEXTILE WASTEWATER	21
3.2.1.	Synthesis of biochar	21
3.2.2.	Synthesis of the photocatalyst composites	22
3.2.3.	Preparation of simulated textile wastewater	24
3.2.4.	Properties of orange II sodium dye	24
3.3.	PHOTOCATALYTIC DEGRADATION OF ORANGE II SODIUM DYE	25
3.4.	ANALYSING TECHNIQUES	26
3.4.1.	Ultraviolet-Visible spectrophotometry (UV-VIS)	26
3.4.2.	Fourier transform infrared spectroscopy (FTIR)	26
3.4.3.	Scanning Electron Microscopy-Energy Dispersive Spectroscopy (SEM-EDS) ...	27
3.4.4.	X-ray diffraction (XRD)	27
3.4.5.	Brunauer–Emmett–Teller (BET)	28
3.5.1.	Effect of catalyst loading	28
3.5.2.	Effect of pH	29
3.5.3.	Effect of initial dye concentration	29
3.5.4.	Kinetics studies	29
3.5.5.	Determination of the electrical Energy Efficiency per order (<i>EE_o</i>)	30
3.5.6.	Reusability of the photocatalyst	31
CHAPTER 4	32
CHARACTERISATION OF THE BIOCHAR, TiO ₂ AND TiO ₂ -SUPPORTED BIOCHAR COMPOSITES	32
4.1.	CHARACTERISATION OF BIOCHAR OBTAINED FROM PJW LEAVES	32
4.2.	UV-VISIBLE SPECTROSCOPY OF THE SYNTHESISED TiO ₂ -SUPPORTED BIOCHAR	36
4.3.	DETERMINATION OF ENERGY BAND GAP TiO ₂ -SUPPORTED BIOCHAR ...	37
4.4.	FTIR ANALYSIS	39

4.5. SCANNING ELECTRON MICROSCOPY ANALYSIS	40
4.6. BRUNAUER EMMET TELLER SURFACE AREA ANALYSIS	41
4.7. X-RAY DIFFRACTION (XRD) ANALYSIS	43
CHAPTER 5.....	45
PHOTOCATALYTIC DEGRADATION OF ORANGE II SODIUM DYE	45
5.1. DETERMINATION OF MOLAR EXTINCTION COEFFICIENT OF ORANGE II SODIUM.....	45
5.2. BATCH STUDY	46
5.2.1. Effect of catalyst loading.....	46
5.2.2. Effect of pH.....	47
5.2.3. Effect of initial dye concentration	49
5.2.4. Kinetics of the photodegradation of orange II sodium dye	51
5.2.5. Electrical Energy Efficiency per order (EE_o) of the photocatalytic degradation of orange II sodium dye.....	54
5.2.6. Photocatalyst reusability.....	55
CHAPTER 6.....	57
CONCLUSIONS AND RECOMMENDATIONS.....	57
6.1. CONCLUSION.....	57
6.2. RECOMMENDATIONS.....	58
REFERENCES.....	59

LIST OF TABLES

Table 2.1:	Nature of water pollution at various stages of processing	6
Table 2.2:	Different processes of advanced oxidation processes AOP	9
Table 2.3:	Summary of previous studies on TiO ₂ -doped carbon band gap	19
Table 2.4:	Summary of previous studies on TiO ₂ -doped carbon band gap	20
Table 3.1:	Characteristic data of orange II sodium	25
Table 4.1:	Yield and chemical compositions of the biochar after varying the pyrolysis times [PJW leaves weight = 10.0 g; temperature = 285 °C]	33
Table 4.2:	Ash content at different times	33
Table 4.3:	Chemical composition of the composites	40
Table 4.4:	The specific surface area and pore structure parameters of TiO ₂ and TiO ₂ -supported biochar composites	42
Table 4.5:	XRD data of TiO ₂ and TiO ₂ -supported biochar composites	43
Table 5.1:	Kinetic parameters of orange II Sodium dye using TiO ₂ and TiO ₂ -supported biochar composites (C _{cat} = 200 mg/L) for 120 minutes at pH 6.8	53
Table 5.2:	Electrical Energy Efficiency per order (<i>EEo</i>) and Kinetic parameters of orange II sodium using the TiO ₂ and TiO ₂ -supported biochar composites at pH 4, 6.8, 8, and 10 [C _{dye} = 20 ppm, C _{cat} = 200 mg/L, time = 120 min, power = 160W] ...	54

LIST OF FIGURES

Figure 2.1:	Schematic illustration of photocatalytic activation in the TiO ₂ on removal of pollutants	11
Figure 2.2:	Impact of doping and photocatalytic mechanism of TiO ₂	12
Figure 3.1:	Flow chart of synthesis of TiO ₂ particles by hydrothermal process	23
Figure 3.2:	Flow chart of synthesis of TiO ₂ -doped carbon by ultrasound process	24
Figure 4.1:	FTIR spectra of PJW leaves and biochars at 1 h, 2 h and 3 h	34
Figure 4.2:	SEM images 10µm: (a) Port Jackson willow leaves (b) biochar at 1 h (c) biochar at 2 h and (d) biochar 3 h	35
Figure 4.3:	XRD pattern of PJW leaves and biochar prepared at 1 h, 2 h and 3h	35
Figure 4.4:	UV-Visible spectra range from (a) 200–550 nm and (b) 300–800 nm for TiO ₂ and TiO ₂ -supported biochar composites	36
Figure 4.5:	Energy band gap (Tauc plots) (a) TiO ₂ and (b) TiO ₂ -supported biochar composites	37
Figure 4.6:	FTIR-spectra of TiO ₂ and TiO ₂ -supported biochar composites	39
Figure 4.7:	SEM images of the (a) TiO ₂ and (b) TiO ₂ - supported biochar composites	40
Figure 4.8:	N ₂ adsorption-desorption isotherm of (a) TiO ₂ and (b)TiO ₂ -supported biochar composites	41
Figure 4.9:	XRD patterns of TiO ₂ and TiO ₂ -supported biochar composites	43
Figure 5.1:	Beer's law plot for orange II sodium dye	44
Figure 5.2:	UV-Visible spectra of orange II sodium dye.....	45
Figure 5.3:	Effect of catalyst loading on the photodegradation efficiency of orange II sodium [C _{dye} = 20ppm, pH = 6.8, time = 60 min]	46
Figure 5.4:	Removal efficiency of the effect of pH on orange II sodium decolourisation, and degradation with (a) TiO ₂ and (b) TiO ₂ -supported biochar composites [C _{dye} = 20 ppm, C _{cat} = 200 mg/L]	47
Figure 5.5:	Effect of pH solution on the photodegradation efficiency of orange II Sodium [C _{dye} = 20 ppm, C _{cat} = 200 mg/L, time = 60 min]	48
Figure 5.6:	Effect of initial concentration on the photodegradation efficiency of orange II Sodium with (a) TiO ₂ and (b) TiO ₂ -supported biochar composites [C _{cat} = 200 mg/L, pH = 6.8]	49
Figure 5.7:	Effect of initial dye concentration on the photodegradation efficiency of orange II sodium. [C _{cat} = 200 mg/L, pH = 6.8, time = 60 min]	50

Figure 5.8:	Plot of $\ln(C_o/C_t)$ versus irradiation time in the degradation of orange II sodium dye using (a) TiO_2 and (b) TiO_2 -supported biochar composites [Ccat = 200 mg/L, pH= 6.8, time = 120 min]	51
Figure 5.9:	Plot of $1/K$ versus dye concentration the degradation of orange II Sodium dye [Ccat= 200 mg/L, pH= 6.8, time=120 min]	52
Figure 5.10:	Reusability of TiO_2 -supported biochar composites for orange II sodium dye degradation for three successive cycles [Ccat = 200 mg/L, Cdye=20 ppm, Time=120 min., pH= 6.8, power= 160W]	55

LIST OF ABBREVIATIONS AND SYMBOLS

AC	Activated Carbon
AOP	Advanced Oxidative Processes
BOD	Biochemical Oxygen Demand
BET	Brunauer–Emmett–Teller
CB	Conduction Band
COD	Chemical Oxygen Demand
EDS	Energy Dispersive Spectroscopy
EDX	Energy Dispersive X-ray
EEO	Energy Efficiency per order
FTIR	Fourier Transform Infra-Red
IAP	Invasive Alien Plan
ICDD	International Centre Diffraction Data
ICP	Inductively Coupled Plasma
IUPAC	International Union of Pure and Applied Chemistry
O&G	Oil & Grease
PJW	Port Jackson willow
PVA	Poly Vinyl Alcohol
ROS	Reactive Oxidizing Species
SEM	Scanning Electron Microscope
TOC	Total Organic Carbon (TOC),
TSS	Total Suspended Solid (TSS),
UV	Ultra-Violet
VB	Valence Band

Keywords: Photocatalytic degradation, textile wastewater, dye, biochar, Acacia saligna.

CHAPTER 1

INTRODUCTION

1.1. BACKGROUND

All essential human activities are directly or indirectly connected with water and the availability of potable water (Pengelly *et al.*, 2017; Ziervogel & Parnell, 2014). Along with the growing population, the water demand is likely to exceed its supply (Samanta, 2019). Thus, extensive funds and scientific research must be focused on water treatment technologies (Enqvist & Ziervogel, 2019).

The textile industry is one of the industries with the greatest water usage in the world with a resultant large amount of wastewater. Consequently, the textile manufacturing company is the second-largest producer of effluent, next to agriculture (Cloete *et al.*, 2010; Greer *et al.*, 2010). Textile wastewater is coloured, which indicates the presence of a variety of dyes that are difficult to remediate (Haroun & Idris, 2009). According to reports, thousands of tons of synthetic dyes are released in the ground water annually. Consequently, the greatest problem in the textile effluent treatment plant is the removal of these coloured dyes (Ajmal *et al.*, 2014; Choudhury, 2018). The presence of dyes in the wastewater causes a severe ecological problem due to their high toxicity (Palter *et al.*, 2006) and capacity for prevention of UV treatment due to their intense turbidity (Saggiaro *et al.*, 2011).

Azo dyes are commonly used in the printing and textile manufacturing industries (Saggiaro *et al.*, 2011). They are harmful when discharged untreated in the environment due to their recalcitrance in common wastewater treatment plants. Their oxidized products are potentially hazardous with recognized carcinogenic and mutagenic aromatic amine constituents (Palter *et al.*, 2006). Azo dyes such as orange II sodium are very stable due to the presence of the azo group (-N=N-) group in their structure (Sandhya, 2010). Their stability and strong colour make it difficult to degrade in the environment, decreasing the quality of water and therefore becoming a source of pollution (Zhang *et al.*, 2011).

Several physical, chemical, and biological technologies or a combination of them can be used for the removal of dyes from wastewater (Lellis *et al.*, 2019). Conventional wastewater treatment, such as adsorption, flocculation, UV treatment, and biological degradation is not effective in their removal due to the high solubility of azo dyes (Sharma & Bhattacharya, 2016). Adsorption

treatment which involves the transfer of pollutants from effluent to an adsorbent that generates waste in the spent adsorbent material, also has limited impact on azo dyes. They are not easily biodegradable and, mostly require specific microorganisms that can endure the toxic mixture of the effluent water (Ezzatahmadi *et al.*, 2018). Advanced oxidative processes (AOP) have been found effective in the treatment of persistent azo dyes pollutants (Ou *et al.*, 2006). They are efficient degradation methods with the promise of complete mineralization of azo dyes economically (Chong *et al.*, 2010; Ezzatahmadi *et al.*, 2018; Badmus *et al.*, 2020). Photocatalytic degradation is prominent as an inexpensive and convenient method that degrade dyes to produce water, carbon dioxide, and harmless inorganic matter (Onyatta *et al.*, 2016). This degradation method is effective as the catalyst can significantly reduce treatment time, improve the efficiency of the process and consequently lower the treatment cost, energy, and time (Lee & Park, 2013).

Among several photocatalytic materials, TiO₂ is very promising due to its strong oxidizing activity, stability, and nontoxicity (Li *et al.*, 2015; Badmus *et al.*, 2021). However, the main disadvantages of TiO₂ are low quantum yields and low solar activity (Stewart, 2018). These setbacks can be overcome by coupling TiO₂ with carbon-based materials such as biochar that improve its photocatalytic activities (Zhang *et al.*, 2017). Biochar can be produced from a variety of carbonaceous raw materials including plant and animal materials. However, plant residues are a particular choice from both economic and environmental standpoints in addition to their abundance (Zhang *et al.*, 2011). In the current investigation, biochar will be prepared through the valorisation process of *Acacia saligna* leaves and its effectiveness as a support using TiO₂ will be investigated. Reactive orange II sodium salt was selected as a framework dye for the examination of the photo-activity of TiO₂-doped carbon composites.

1.2. PROBLEM STATEMENT

Azo dyes are the most used synthetic dyes in the textile industry (Ohashi *et al.*, 2012). Their high stability and the presence of aromatic rings in their structures complicate the treatment by biodegradation processes (Singh *et al.*, 2016). Common methods used in the degradation of azo dyes are disadvantageous due to the extensive treatment time and by-products that are carcinogenic. Besides, the produced toxic aromatic amines can constitute a danger for the nearby population and environment (Ajmal *et al.*, 2014). Heterogeneous photocatalysis processes have been demonstrated to be efficient in the degradation of azo dyes (Onyatta *et al.*, 2016). The challenge is in the application of an effective and environmentally friendly photocatalyst that

ensures the complete mineralization of azo dyes. The photo-activity of TiO₂ is low due to its large energy band gap which leads to poor solar activity. Supporting TiO₂ with a non-metal, such as biochar can enhance the photocatalytic activity of TiO₂ in the visible region and enable the utilization of a larger amount (greater than 45 %) of solar energy.

1.3. AIM AND OBJECTIVES

Degradation of orange II sodium dye in textile wastewater using simulated solar-light in the presence of TiO₂-supported biochar composites.

The aim of this research will be achieved through the following objectives:

- Synthesis and characterisation of biochar from *Acacia saligna* leaves;
- Synthesis and characterisation of TiO₂ from TiCl₃ as precursor;
- Synthesis and characterisation of TiO₂-supported biochar;
- Application of the synthesized TiO₂ and TiO₂-supported biochar composites for the decolouration of reactive orange II sodium dye solution;
- Determination of the effect of some reaction parameters such as the catalyst loading, pH, and initial concentration of dye.

1.4. RESEARCH QUESTIONS

- Can biochar be synthesized from *Acacia saligna* leaves?
- Can TiO₂ be synthesized using TiCl₃ as a precursor?
- Can TiO₂ be supported on the synthesized biochar from *Acacia saligna* leaves?
- Can the synthesized TiO₂-supported biochar composite be applied for the decolouration of reactive orange II sodium dye solution?
- What are the effects of pH, time, temperature, catalyst loading, and initial concentration of dye in the degradation process?

1.5. SIGNIFICANCE OF THE RESEARCH

The synthesis of TiO₂-supported biochar composite will enable the optimum utilization of solar-light through the energy band gap reduction.

1.6. DELINEATION

This study will only focus on the synthesis of TiO₂-supported on biochar of *Acacia saligna* leaves and its application for the photocatalytic degradation of simulated textile wastewater (orange II sodium salt). The Photochemical degradation using raw wastewater will not be carried out during the current investigation.

1.7. RESEARCH ASSUMPTIONS

- TiO₂-supported biochar nanocomposite will show activity in the visible light region.
- The photocatalytic activity of TiO₂ will be enhanced by the presence of biochar.
- The application of TiO₂-supported biochar composite will lead to the degradation of wastewater under ultraviolet radiation.

CHAPTER 2

LITERATURE REVIEW

This chapter contains the literature reports on textile wastewater, its impact on the environment, and conventional methods used in their treatment. It also focuses on Advanced Oxidative Processes (AOPs) and heterogeneous photocatalysis using TiO₂ in water treatment, and possible techniques in the modifications of TiO₂. An overview of biochar used as support in photocatalysis is given.

2.1. CHARACTERISTICS OF TEXTILES WASTEWATER

Textile effluents contain a large number of dyes such as azo dyes (Saggiaro *et al.*, 2011) and other organic pollutants. It poses a real threat to the environment due to their characteristics colour (Ahmed *et al.*, 2007), high temperature (Kumar, 2016), fluctuating pH, malodour (Mahlambi *et al.*, 2015), COD, BOD, TOC, TSS, O&G, inorganic heavy metals such as Cu, Ni, Zn, Cr, Cd, As, Fe, and Pb, microbial impurities, and others organic substances including pesticides, phenols, phosphates, and surfactants (Ghaly *et al.*, 2013; Anjum *et al.*, 2017; Fluence News Team, 2019). Table 2.1 below illustrates the nature of wastewater pollutants at different stages of textile processes (Laxman, 2009).

2.2. TEXTILE DYES

Textile dyes are soluble and non-biodegradable coloured organic compounds with their complex chemical structure which contains various chromophoric fractions, e.g. -C=O, -C=C-, -N=N-, -NO₂, -C=N-, etc. (Palter *et al.*, 2006, Lellis *et al.*, 2019). Dyes can be obtained from natural materials such as minerals, plants, animals, and microorganisms and can also be synthesized (Saggiaro *et al.*, 2011). Synthetic dyes are categorized into azoic, basic, metal complex, optical brightener, and sulfur dyes. Azoic dyes, also known as azo dyes, and basic dyes are considered the most hazardous due to the high toxicity of their components and breakdown products (Hassaan & Ahmed, 2017). However, azo dyes are extensively used in the industry due to their low cost (Ozer & Kevser, 2010).

Table 2.1: Nature of water pollution at various stages of textile processing

Process	Possible pollutants	Nature of effluent
Desizing	Fats, resins, starch, waxes, glucose and PVA do not utilize a high BOD.	Very small amount, PVA, and high BOD.
Kiering	Fragments of cloth, soda ash, caustic soda, waxes and sodium silicate.	Very small amount, strongly alkaline, dark colour, and high BOD.
Bleaching	Acids, caustic soda, chlorine, hypochlorite, hydrogen peroxide.	Small amount, strongly alkaline, and low BOD.
Mercerizing	Caustic soda.	Small amount, strongly alkaline, and low BOD.
Dyeing	Mordants, dyes, and reducing agents like soap, acetic acid and sulphides.	Large amount, strong colour, and fairly high BOD.
Printing	Mordants, dyes, china clay, acids, gum oil, metallic salts, and starch.	Very small amount, oily appearances, and fairly high BOD.
Finishing	Salts, traces of starch, waxes, traces of starch, etc.	Very small amount, softly alkaline, and low BOD.

Azo dyes are mostly synthetic dyes with a complex structure consisting of conjugated double bonds and aromatic amine rings (-N=N-) (Sandhya, 2010). This structure permits intense π - π^* transitions in the UV-visible region, with high extinction coefficients (Khan & Banerjee, 2010). They are xenobiotic with high solubility and low biodegradation. Their toxicity (genotoxicity, mutagenicity, and carcinogenicity) is due to their degradation products such as aromatic amines (Brown & DeVito, 1993). Azo dyes can also contain heavy metals and recalcitrant organic molecules, which are resistant to microbial treatment, very stable to oxidizing agents and light. They are classified as hazardous pollutants and may harm human health (Eletta *et al.*, 2018; Guo *et al.*, 2010). The effects of azo dyes on public health depend mainly on the length and route of exposure, the number of dyes as well as the relative toxicity of the dyes (Ki-Hyun *et al.*, 2013). Generally, the common danger of azo dyes is a lung disease, caused as a result of the breathing

of dye particles. This is known as respiratory sensitization (Hassaan, 2016; Hassaan & Amhed, 2017). The removal of azo dyes from the environment must be prioritized for public safety.

2.3. CONVENTIONAL TREATMENT OF AZO DYES IN TEXTILE WASTEWATER

Conventional techniques employed for textile dyes treatments are following (Chandran, 2015):

- **Physical methods** such as aeration, degasification, equalization, filtration, flotation, screening, sedimentation, and skimming.
- **Chemical methods** such as adsorption, chlorination, coagulation, neutralization, and ozonation.
- **Biological methods** can be aerobic processes (such as activated sludge treatment methods, aerobic digestion, lagoons, ponds, Trickling filtration, and oxidation) or anaerobic processes (such as lagoons, anaerobic digestion, and septic tanks)

These conventional treatments of textiles wastewater can be categorized into primary, secondary, and tertiary treatment processes, and are very common in the production of potable water (Ghaly *et al.*, 2013).

2.3.1. Primary treatment

The primary treatment consists of a physicochemical pre-treatment that is meant to eliminate several refractory COD with the separation of dye effluents (Shyan *et al.*, 2007; Chandran, 2015). Some primary treatment methods are screening, sedimentation, homogenization, neutralization, and mechanical-chemical flocculation (Vineta *et al.*, 2014).

2.3.2. Secondary treatment

The secondary treatment involves biological treatment. Biological treatment, also known as conventional activated sludge systems can eliminate a huge amount of COD (Wang *et al.*, 2011). Biological processes can be anaerobic or aerobic. Coupled anaerobic-aerobic treatment may be

applied in the treatment of azo dyes without their complete degradation due to the increasing presence of molecules in the wastewater (Guo *et al.*, 2010; Chandran, 2015). Industrial wastewaters are generally treated by biological treatments such as oxidation ditch and pond, anaerobic and aerobic digestion, trickling filtration, and aerated lagoon (McMullan *et al.*, 2001; Fu & Viraraghavan, 2001).

2.3.3. Tertiary treatment

The tertiary treatment consists of a combination of biological and physicochemical treatment, which were developed to treat recalcitrant pollutants (Wang *et al.*, 2011). Tertiary treatment can be effective in the removal of dyes by reducing high concentrations of colour from the effluent (Chandran, 2015). Some wastewater tertiary treatments include processes such as oxidation techniques, membrane–filtration processes, electrochemical processes, thermal evaporation, and ion exchange process (Huang *et al.*, 2011).

Conventional techniques applied to treat textile wastewater are mostly inadequate due to the presence of highly toxic reactive compounds such as aromatic components of dissolved organic compounds, such as azo dyes. Therefore, more advanced techniques such as advanced oxidative processes (AOP) must be used to decolorize and reduce recalcitrant wastewater loads (Nova *et al.*, 2009; Hassaan & Nembr, 2017).

2.4. ADVANCED OXIDATIVE PROCESSES (AOPs)

Advanced oxidative processes (AOPs) are non-conventional but effective methods that can treat recalcitrant organic compounds dissolved in wastewater as they can completely degrade these compounds into water, carbon oxide, and harmless inorganic substances (Mahlambi *et al.*, 2015). AOPs may as well be used as a pre-treatment to decrease the concentrations of toxic pollutants followed by biological wastewater treatment processes (Garrido-Cardenas *et al.*, 2019). AOPs include all the catalytic and non-catalytic processes that exploit the high effectiveness of the hydroxyl radical (OH[•]) used as a strong oxidant for the formation of harmless by-products (Hassaan & Nembr, 2017). These methods use compounds such as O₃, H₂O₂, transition metals, and metal oxides as a precursor of OH[•] with catalysts (including metal oxides and transition metals) and energy (such as ultraviolet, visible, electronic current, γ -radiation and ultrasound) (Stasinakis,

2008; Studies, 2011). AOPs can use homogeneous or heterogeneous catalysts. In homogeneous catalysis, photocatalysts, and reactants are in the same phase. It is very difficult to disassociate the photocatalyst from the product in homogeneous catalysis. This can lead to thermal decomposition of the photocatalyst. Meanwhile, in heterogeneous catalysis, the reactants (generally liquid or gas) and photocatalyst (solid) are in a different phase. The photocatalyst is accessible and at the end of the reaction, the photocatalyst and its by-products are easily separated (Ranga, 2017). Table 2.2 illustrates the classification of advanced oxidation processes (Mota *et al.*, 2008).

Table 2.2: Different processes of advanced oxidation processes AOPs

Types of AOPs	Homogeneous processes	Heterogeneous processes
Non- photochemical	<ul style="list-style-type: none"> - Electro-oxidation - Electrohydraulic discharge – ultrasound - Fenton ($\text{Fe}^{3+}/\text{H}_2\text{O}_2$ or Fe^{2+}) - Ozonation with $\text{O}_3/\text{H}_2\text{O}_2$ - Ozonation in alkaline media (O_3/HO^-) - Supercritical water oxidation (SCWO) - Wet air oxidation (WAO) 	Catalytic wet air oxidation (CWAO)
Photochemical	<ul style="list-style-type: none"> - Photo-Fenton (Fe^{2+} or $\text{Fe}^{3+}/\text{H}_2\text{O}_2/\text{UV}$) - Photolysis of water in vacuum ultraviolet (VUV) - $\text{UV}/\text{O}_3/\text{H}_2\text{O}_2$ - $\text{UV}/\text{H}_2\text{O}_2$ - UV/O_3 	Heterogeneous photocatalysis: TiO_2/UV , $\text{TiO}_2/\text{H}_2\text{O}_2/\text{UV}$, SnO_2/UV , ZnO/UV .

Heterogeneous photocatalytic using TiO_2 processes are extensively used for wastewater treatment because of their higher effectiveness and large potential for the degradation of recalcitrant pollutants and deadly bacteria (Donga *et al.*, 2015; Ranga, 2017).

2.5. HETEROGENOUS PHOTOCATALYSIS

Heterogeneous photocatalysis is a treatment based on the photo-activation of semiconductor nanoparticles (for example SiO₂, TiO₂, Al₂O₃, ZnS, etc.) by visible light irradiation that generates reactive oxidizing species (ROS) which can cause the degradation of organic pollutants (Pelaez *et al.*, 2012). The photo-activation of nanomaterials is the transition at an ambient temperature of an electron (e^-) from the valence band (VB) to the conduction band (CB) due to the absorption of photons having equal or higher energy than the band gap energy (Nova *et al.*, 2009). This absorption generates oxidizing sites known as holes, h^+ , in the valence band that reacts directly using pollutant or indirectly using wastewater generating OH \cdot . While in the conduction band, the electron reduces the oxygen accumulated on the surface of the nanoparticle (Gautam & Chattopadhyaya, 2017). This process can lead to the total degradation of toxic pollutants to harmless species such as carbon dioxide and water (Rashed *et al.*, 2017).

Titanium dioxide, TiO₂ is the ideal semi-conductor nanoparticle used in the photocatalytic process due to its thermochemical stability, low price, availability, high reactivity under light irradiation, and low toxicity (Zhang *et al.*, 2017). The high chemical stability of TiO₂ is one of the major advantages that make the heterogeneous photocatalysis a semi-permanent process in the degradation of dyes (Kursvuran *et al.*, 2005). However, TiO₂ shows photo-physical limitations due to the large energy band gap (2.8 - 3.2 eV) of pure TiO₂. It can only be active within the UV spectrum which is less than 5 % of the solar light (Kanakaraju *et al.*, 2014). Overcoming these issues will facilitate the utilization of natural sun light for textile wastewater remediation (Donga *et al.*, 2015). Moreover, it can be done by modifying the TiO₂ with a compound like a metal, non-metal, etc., that has a larger surface area. The surface area of the compound should be large enough to support which promotes high photocatalyst distribution and increase of the active sites (de Oliveira *et al.*, 2019).

The mechanism of photocatalytic activation in the TiO₂ and the degradation of pollutants by the photocatalytic activity of TiO₂ are demonstrated in Figure 2.1 (Moyet, 2019) and as shown below (Gautam & Chattopadhyaya, 2017):

- Activation of TiO₂ by light radiation



This equation shows the subjection of TiO₂ to UV light in a water solution.

- **Degradation of pollutants by the photocatalytic activity of TiO₂**

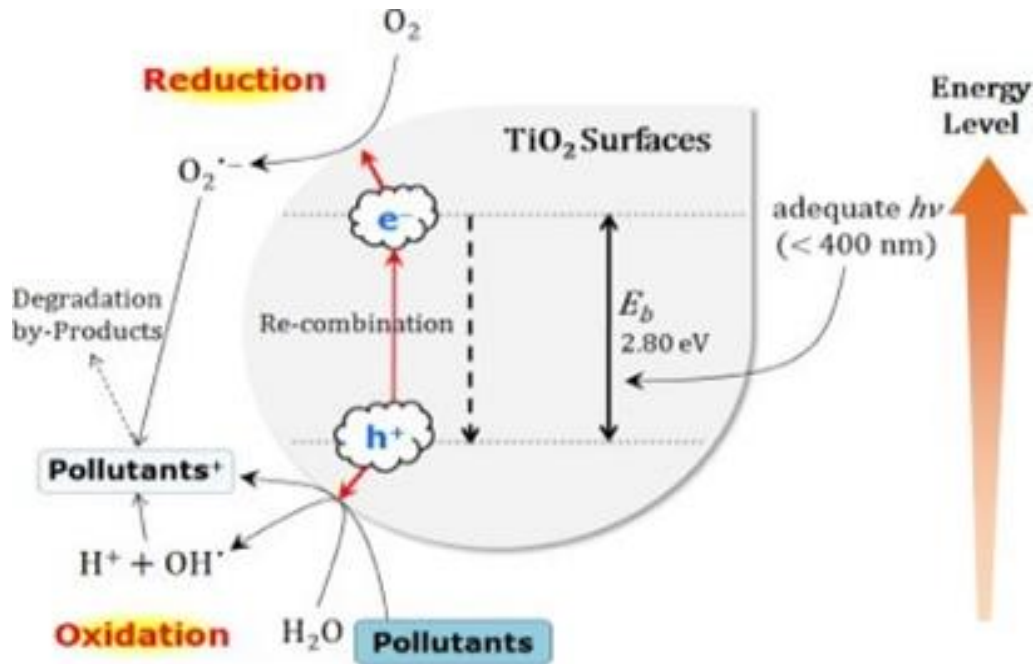
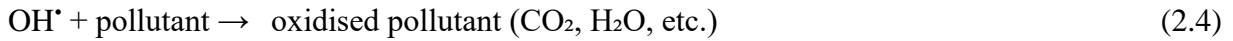


Figure 2.1: Schematic illustration of photocatalytic activation in the TiO₂ on the removal of pollutants (Moyet, 2019).

2.6. TiO₂ MODIFICATIONS

The principal objective of TiO₂ modifications is to reduce its energy band gap thus moving its optical response from the UV to the visible region and reducing the electron-hole pair recombination. Several modifications techniques including doping with metals and non-metals, dye sensitization, deposition with noble metals, and coupled semiconductors have been applied. However, studies show that doping has a positive effect on TiO₂ because it introduces elements such as metal and non-metal in the titania structure that lead to the increase of its photo-activity

by changing the functional properties of the TiO₂ (Wei *et al.*, 2008; Wong *et al.*, 2008; Mahlambi *et al.*, 2015). Figure 2.2 demonstrates the effect of doping and the photocatalytic process of TiO₂.

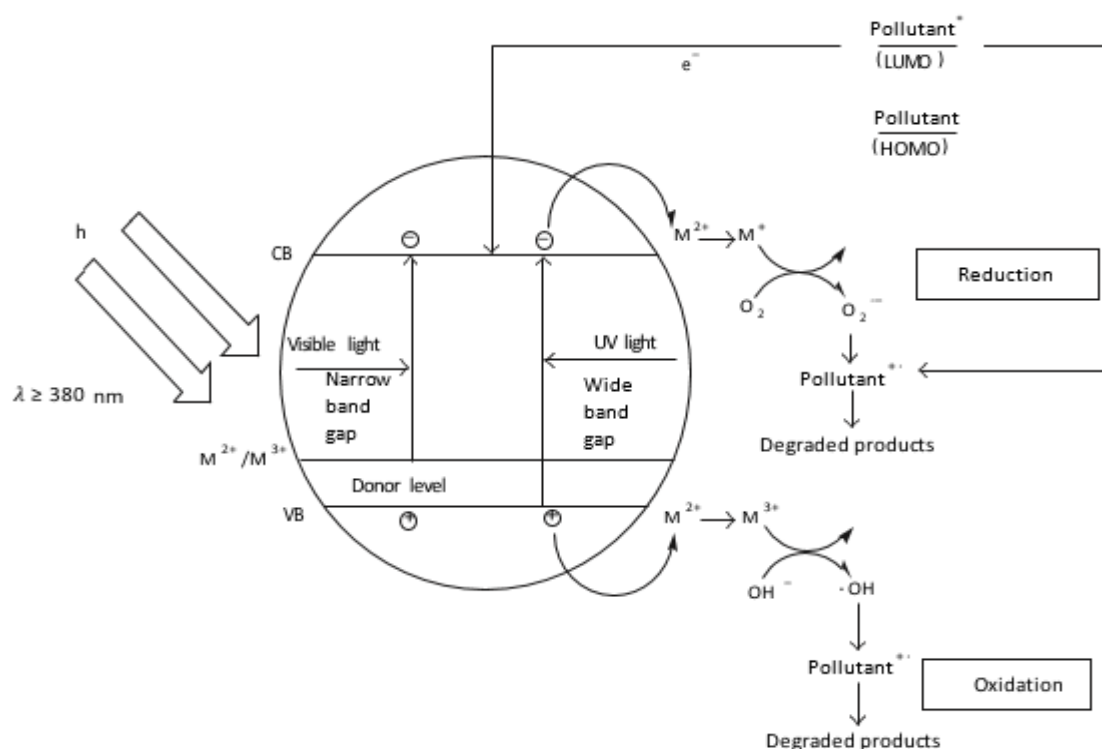


Figure 2.2: Impact of doping and photocatalysis process of TiO₂ (Hoffmann *et al.*, 1995).

The impact of doping in the photocatalyst is regulated by factors, such as the nature of the dopant, the synthesis process, and the physicochemical properties of the photocatalyst. Various ways of increasing the photo-activity of TiO₂ are mentioned below.

2.6.1. Non-metal doping

TiO₂ supported with a non-metal (such as C, F, B, S, Cl, N, and Br) has been considered as second-generation photocatalysts. Studies show that modifying TiO₂ with a non-metal may inhibit the electron-hole pair recombination (Wang *et al.*, 2011, Zhang *et al.*, 2011). Lately, doping with non-metal, such as C, I, F, S, P and N, has been widely investigated due to their relatively high photoelectric properties and photocatalytic stability that may modify the electronic structure of the TiO₂ (Kang *et al.*, 2019). However, compared to the metal-doped TiO₂, the purpose of the non-metal doped TiO₂ is to decrease the recombination of electron-hole pairs. In

this doping, oxygen atoms are substituted by the non-metal in the TiO₂ lattice, which may greatly reduce the band gap and therefore increase the visible light response of TiO₂ (Muhich *et al.*, 2014; Kang *et al.*, 2019). Notably, non-metal doping at the atomic grade can maintain the intrinsic surface properties of the TiO₂, as the dopant act as an isolated particle instead of clusters throughout the surface (Donga *et al.*, 2015). Moreover, the exceptional distribution of dopant states is usually found nearly over the VB maximum, making the photo-generated holes on these states oxidative enough for further photo-reactions (Mahlambi *et al.*, 2015).

2.6.2. Metal oxide doping

Doping with more than one metal oxide such as ZrO₂, WO₃, Fe₂O₃, SnO₂, Ln₂O₃, RuO₂ may lead to the enhancing of TiO₂ photocatalytic effectiveness and inducing the diminishing of the band gap by causing a structure modification into the TiO₂. Therefore, the photocatalytic activity is increased and the metal oxides expand the TiO₂ surface (Mahlambi *et al.*, 2015). However, some of the metal oxides are thermodynamically unbalanced, for instance, RuO₂/TiO₂, thus causing the electron-hole pair recombination and greatly reducing the photo-activity (Beydoun & Amal, 2002).

2.6.3. Metal-ion doping

The modification of TiO₂ with transition and noble metal including Pt, Au, Ag, Cu, V, Ni, and Sn has been found to increase the photo-response and photocatalytic activity of TiO₂ into the visible-light region (Donga *et al.*, 2015). Metal-ion doping can lead to the duplication of the CB in TiO₂ with the *d*-orbital of the transition metal, that produces the decrease in the energy band gap (Mahlambi *et al.*, 2015). It leads to the creation of new energy levels between the VB and CB with electron transfer due to light absorption into the visible light region. Transition metal ions can also play the role of recombination sites for the photo-induced charge carriers, therefore, decreasing the quantum effectiveness (Ghasemi *et al.*, 2009; Mahlambi *et al.*, 2015).

Metal-ion doping may enhance the rate of centre recombination and generate thermal imbalance. It is therefore essential to prevent this by considering the effective quantity of the metal-ion during the synthesis of the doped TiO₂ composites. Although the metal-ion level crosses the optimum limit (at a very low concentration), it acts as the recombination centres for charge

carriers by causing photo-activity. The existence of an acceptable quantity of metal-ion doping (optimum limit) guarantees that the metal particles simply appear as electron traps thus helping electron-holes split (Gorska *et al.*, 2008).

2.7. PORT JACKSON WILLOW (*ACACIA SALIGNA*)

The Port Jackson Willow (PJW) is a flexible tree that grows rapidly in semi-desert regions (including South Africa) as windscreens and as an ornamental tree (Cronk & Fuller, 1995). It has become an invasive species outside of its natural range, therefore threatening biological diversity and is categorized as an Invasive Alien Plan (IAP). IAP harms the ecosystem by consuming more water than local plants, exhausting valuable water resources, and also providing material for wildfires, making them exceptionally hot, which destroys the soil structure and sterilise the soil for up to three years (Richardson & Kluge, 2008). This results in negative ecological, social, and economic impacts. As we depend on biodiversity for water, food, wood, clean air, medicine, and much more, we must protect this resource.

2.7.1. Identification of the Port Jackson Willow

PJW is a sprout that grows in sandplain, near rivers, wetlands, and on the coastal plain where there is a high-water table. The bark of young plants or new branches is smooth and greyish, but as the plant grows older, it darkens and cracks. This plant has long, slender blue-green phyllodes that look like leaves. The phyllodes measure around 1 to 5 cm large and 20 cm long with one clear midrib. (Hildegard, 1987). Such phyllodes make the tree appear as a willow tree while it is truly an acacia tree. The PJW generates bouquets of shining yellow flowers such as tiny pom-poms from Spring to midsummer. The thin, linear shucks are brownish with a neutral border, and little bound among the seeds. They fall off the plant after releasing the shiny dark brown seeds.

2.7.2. Invasion of the Port Jackson Willow in South Africa

Port Jackson Willow was brought from Australia to South Africa for dunes stabilization, animal foods, and a source of woods, also because its peels entered into the process of tanning leather and for ornament (Cronk & Fuller, 1995; Midgley & Turnbull, 2003). The PJW is a persistent

seed bank, that is expanded by a stream and enfolded by local ants, that may rapidly uproot after a fire or rain due to its impermeable seed dormancy ability (Richardson & Kluge, 2008). The seeds may also be distributed when sand for roads, buildings etc., is transported from quarries or riverbanks where these trees are numerous (Hildegard, 1987). The Port Jackson willow quickly invaded offshore and stream areas (Cronk & Fuller, 1995).

PJW crops can grow in poor and calcareous soil because their roots contain symbiotic bacteria that catch Nitrogen gas from the air and turn it into fertilizer for the plant. It has been listed as an invasive alien plant in the Cape Floristic Region of South Africa, where it has displaced native species through changing fire regimes (Richardson *et al.*, 2004).

2.8. SYNTHESIS OF BIOCHAR (CARBON)

Biochar is a solid carbonaceous material with stable sequestration (Kuzyakov *et al.*, 2009). Research has shown that biochar may be used as a cost-effective sorbent in the removal of pollutants in wastewater due to the chemical groups (-COOH, COO-, -C=O, -C=O, -OH, etc.) present on its surface (Zhang *et al.*, 2012; Oliviera *et al.*, 2021). Biochar is an excellent platform for supporting various metal oxides catalytic nanoparticles due to its high surface energy with a controlled pore size (Mahlambi *et al.*, 2015), easy tuneable functional groups, chemical stability, strong magnetic attraction (Mian & Liu, 2018) easy availability, and simplicity of operation (Nguyen *et al.*, 2020). Biochar can also improve the reactivity of the nanomaterial by increasing the surface area and the number of active sites of the metallic nanoparticles and also ameliorate the charge separation of the e^-/h^+ pair during the photocatalysis (Mian & Liu, 2018); which, consequently, enhances the photodegradation of organic pollutants (Kang *et al.*, 2019). However, the proprieties of biochar are determined by the characteristics of the precursor (biomass) for example the size, density, rigidity, and percentage of the ash and its composition (Spokas *et al.*, 2012).

Biochar is a product of pyrolysis of renewable and sustainable carbon-based material (biomass) such as plant and animal materials used as precursors. Pyrolysis is the thermochemical degradation of biomass happening in the absence supply of oxygen. The process depends on factors including thermal environment (from 200°C to 700°C), yielding materials with their chemical composition (Oliviera *et al.*, 2021), moisture, particles size (Salman, 2020), rate of heating, and removal time (Zhang *et al.*, 2011). The pyrolysis temperature is one of the most important parameters that influence the proprieties of the final product (Oliviera *et al.*, 2021).

Pyrolysis processes can be categorized as torrefaction (200°C – 320°C) and produce materials of amorphous carbons predominance, slow pyrolysis (350°C – 700°C) that takes several hours and fast pyrolysis (450°C – 550°C) that takes minutes to complete the process and is mostly used (Spokas *et al.*, 2012). Above the temperature of 700°C, carbonization with oxygen and hydrogen elimination occurs leading to the formation of carbon material with a higher amount of aromatic structures (Oliviera *et al.*, 2021).

2.9. SYNTHESIS OF TiO₂-SUPPORTED BIOCHAR COMPOSITES

The processes used for the synthesis of TiO₂-supported biochar composites are mentioned below:

2.9.1. Sol-gel process

The sol-gel method is a process in which a Sol (liquid) changes gradually to a Gel (solid phase). Sol is a colloidal solution in which particles are in suspension in a liquid. And a gel is a semi-solid material with a three-dimensional continuous system, that is enveloped in a liquid (Kumar, 2018). This process is used for the deposit of TiO₂ composites on the surface of biochar (Rashed *et al.*, 2017) and is done as follow :

- (1) Pyrolysis of Biomass to obtain biochar;
- (2) Acid treatment to increase the surface area of biochar followed by TiO₂ deposition on the surface of biochar; and finally.
- (3) Heat treatment of TiO₂-supported biochar to obtain a composite with a stable structure (Mian & Liu, 2018).

2.9.2. Solvothermal process

The solvothermal method is the hydrothermal synthesis of composites at a wide range of temperature (from 100°C to 1000°C) and pressure (from 1 atm to 10 000 atm) in a solvent with high boiling points (such as ethanol) without changing the nanomaterial composition (Kumar, 2018). The solvothermal process is done as follow:

- (1) The deposition of TiO₂ onto biochar, then mix with an ethanol solution.

- (2) The mixture was placed into a Teflon-lined stainless-steel autoclave, followed by a solvothermal treatment overnight.
- (3) The resulting powder was washed, dried, and calcined to obtain TiO₂-supported carbon composites (Mian & Liu, 2018).

2.9.3. Sonochemical process

The sonochemical synthesis is the preparation or modification of inorganic composites with high-surface-area by using sonochemistry principles (Gong & Hart, 1997) and is done as follows: Firstly, biochar was prepared via thermal decomposition of biomass, then the obtained biochar was mixed with TiO₂ in the presence of a solvent (for-example ethanol) follow by sonication of the mixture. After sonication, the solvent was then removed via a rotary vacuum evaporator. Finally, the obtained material was dried and calcined to obtain TiO₂-supported biochar composite (Mian & Liu, 2018).

2.10. TiO₂-SUPPORTED CARBON COMPOSITES IN PHOTOCATALYSIS

Extensive studies have been done on the photo-activity of TiO₂-supported carbon composite in the degradation of organic pollutants. Azo dyes are one of the most studied pollutants in photocatalytic degradation, due to their large utilization in the industry (e.g. textile industry) and their harmful properties including mutagenic and carcinogenic effects and may negatively impact on before human health and the environment (Castro *et al.*, 2019; Chiu *et al.*, 2019).

Subramani *et al.* (2007) studied the degradation of indigo carmine dye using TiO₂-impregnated activated carbon nanocomposites under 8 W UV lamps. Their result revealed that the initial concentration of the dye and amount of the catalyst can greatly affect photocatalytic performance. The mineralization of the dye was revealed by the reduction in COD. Singh *et al.* (2016) studied the degradation of direct blue 199 dye using activated carbon-based TiO₂ composites under a 196 W mini lamp. They also studied the reaction kinetic modeling of the photocatalytic, sonocatalytic, and sono-photocatalytic processes. Their results showed that the sono-photocatalytic process showed maximum degradation. However, the photocatalytic reactor was more efficient as it consumed less energy. They also demonstrated that the degradation reactions of direct blue 199 followed the Langmuir–Hinshelwood model.

Xing *et al.* (2016) studied the degradation of rhodamine B using activated carbon-based TiO₂ composites under a 450 W high-pressure mercury lamp. They also investigated the effect of loading cycles of TiO₂ on the structural properties. The results indicated that after multiple loading cycles the porosity of TiO₂/AC composites decreased and the dispersibility of TiO₂ particles on the AC surface becomes less uniform. The highest photocatalytic activity was observed after 2 loading cycles.

Rashed *et al.* (2017) studied the adsorption and photocatalysis of TiO₂/sewage sludge-based activated carbon composites for the removal of methyl orange and Cd in wastewater using a 15 W UV irradiation lamp. They also investigated the parameters affecting the photocatalytic process such as solution pH, TiO₂: sewage sludge-based activated carbon ratios, nanocomposite dosage, UV irradiation time, and initial pollutant concentrations. Their results showed that these factors have a direct effect on photocatalysis efficiency.

Zhang *et al.* (2017) reported the adsorption and photocatalysis degradation of acid red 18 using ordered mesoporous TiO₂-doped activated carbon under an ultraviolet lamp. They also studied the kinetic model. They reported that the adsorption and photocatalytic degradation followed the pseudo-second-order kinetic model. The complete mineralization of dyes might have occurred due to the presence of strong oxidizing free radicals provided by M-TiO₂.

Nguyen *et al.* (2020) studied the kinetics of adsorption and photocatalysis in the removal of phenol, naphthol blue-black, and reactive black 5 under UV lamps. Their kinetic analysis revealed that the adsorption-assisted photocatalysis performance depended on the similarity of the initial rates of adsorption and degradation determined by the properties of the photocatalyst and the dye.

Mondol *et al.* (2021) synthesised activated Carbon/TiO₂ nanohybrids by hydrothermal technique. They investigated the photocatalytic activity of activated carbon/TiO₂ nanohybrids by degradation of Reactive Red-35 dye using solar irradiation in open-air. Their report showed that the photodegradation was mainly controlled by the radicals $\cdot\text{OH}$ and $\cdot\text{O}_2^-$. The photocatalytic performance was significant due to the synergistic effect of adsorption and photodegradation activity of the nanohybrids.

The Table 2.3 gives previous research done on the synthesis of TiO₂-doped carbon composites and their energy band gap. It can be noted that most of these reports show a decrease in band gap and therefore enhance the photocatalytic activity of TiO₂.

Table 2.3: Summary of previous studies on TiO₂-doped carbon band gap.

Photocatalyst	Band gap (eV)	Reference
Carbon modified TiO₂	2.60	Chao <i>et al.</i> , 2009
Carbon-doped mesoporous TiO₂	2.77	Hu <i>et al.</i> , 2013
Carbon-doped Titanium	2.44	Wei <i>et al.</i> , 2014
C-doped Titania film	2.02	Klaysri <i>et al.</i> , 2017
TiO₂ / C-dot	3.10	Syafei <i>et al.</i> , 2017
Carbon-doped TiO₂	2.20	Sarunas <i>et al.</i> , 2019
Carbon-doped TiO₂	2.82	Cheol <i>et al.</i> , 2021
C-doped TiO₂	2.71	Au-pree <i>et al.</i> , 2021

The synthesis of TiO₂-supported carbon composite has been reported as enhancing the photocatalytic activity of TiO₂ and is effective for dye removal in wastewater. Table 2.4 below shows several studies on the photocatalytic performance of TiO₂-doped carbon composites done in the removal of azo dyes.

Table 2.4: Summary of extensive researches on photocatalytic degradation of reactive dyes using TiO₂-doped Carbon nanoparticles.

Photocatalyst	Biomass	Pollutant	Degradation Efficiency	Synthesis method	References
TiO₂-impregnated AC	Commercial AC	Indigo Carmine	91.06 %	Hydrothermal	Subramani <i>et al.</i> , 2007
TiO₂/AC	Rice husk	Direct blue 199	92 %	Sol-gel	Singh <i>et al.</i> , 2016
TiO₂-doped AC	Lignite	Rhodamine B	93.20 %	Sol-gel	Xiang <i>et al.</i> , 2016
TiO₂/Sewage Sludge-based activated carbon	Sewage Sludge	Methyl orange	94.28 %	Sol-gel	Rashed <i>et al.</i> , 2017
TiO₂/AC	Wallut Shell	Acid red 18	92.30 %	Sol-gel/ Ultrasound	Zhang <i>et al.</i> , 2017
TiO₂/AC	Commercial AC	Naphthol blue black Reactive black 5	90 % 85 %	Hydrothermal	Nguyen <i>et al.</i> , 2020
AC/ TiO₂ nanohybrids	Commercial AC	Red-35	95 %	Hydrothermal	Mondol <i>et al.</i> , 2021

CHAPTER 3

METHODOLOGY

This chapter gives a detailed account of the experimental procedures followed to attain the objectives of this study regarding the photocatalytic degradation of orange II sodium dye in textile wastewater.

3.1. CHEMICAL REAGENTS AND MATERIALS

All the chemicals used in this research for the preparation of photocatalyst composites and simulated textile wastewater, including hydrochloric acid solution ($\geq 37\%$), nitric acid solution ($\geq 65\%$), ethanol ($\geq 99\%$), titanium (III) trichloride solution ($\geq 12\%$), and orange II sodium salt ($\geq 85\%$), were obtained from Merck and Sigma Aldrich. Deionised water in milli-Q water ($18\ \Omega\ \text{cm}$). Port Jackson Willow leaves were used as raw material for the preparation of Biochar.

3.2. PREPARATION OF PHOTOCATALYST NANOCOMPOSITES AND SIMULATED TEXTILE WASTEWATER

3.2.1. Synthesis of biochar

The Biochar was prepared by pyrolysis of the Port Jackson Willow leaves. The leaves were washed multiple times with deionised water to eliminate impurities such as dust, then dried and ground. 10.0 g of the dried powdered leaves was put in a Teflon crucible and placed in an oven at 285°C at a different time ranging from 1 hour to 3 hours to obtain biochar.

The yield of the biochar was obtained after the carbonization of the PJW leaves in the oven. The percentage of biochar yield was calculated from the following equation (Sadaka *et al.*, 2014):

$$yield = \frac{m(\text{biochar})}{m(\text{raw})} \times 100 \quad (3.1)$$

Where *yield* is the mass yield of biochar (%), *m(biochar)* is the masse of obtained biochar (g), *m(raw)* is the masse of raw biomass (g).

The ash content was obtained as follows: 5 g of the dried sample was put in a crucible and placed in the muffle furnace for 20 hours at 570°C.

Calculation of percentage of the ash-based on formula (Nielsen, 2010):

$$\% = \frac{\text{weigh after ashing} - \text{tare crucible weigh}}{\text{original sample weigh}} \quad (3.2)$$

3.2.2. Synthesis of the photocatalyst composites

TiO₂ composites were synthesised by a hydrothermal method (Joni *et al.*, 2018) and TiO₂-supported biochar composites were obtained from the mixing of TiO₂ and biochar using an ultrasound method.

3.2.2.1. Synthesis of TiO₂ composites

TiO₂ composites were synthesised using a hydrothermal process with TiCl₃ as a precursor (Figure 3.1). Firstly, 7 ml of TiCl₃ were added to 1.5 ml concentrated HCl and 9 ml of distilled water (used as a solvent) and stirred for 15 minutes. The resultant solution was put in a water bath at 80°C for 10 minutes before slowly adding 6 ml of concentrated HNO₃ as the reaction is highly exothermic. The heating was then continued for 4 h, 6 h, 8 h, and 10 h. The resultant titanium solution was then washed multiple times via centrifugation with distilled water to remove the excess acid and put in a desiccator.

3.2.2.2. Synthesis of TiO₂-supported biochar composites

TiO₂-supported biochar composites were obtained using an ultrasound process by the mixing of TiO₂ synthesised from TiCl₃, biochar at different ratios (2:1, 2:2, 2:3, and 2:4), and 10 ml of

ethanol used as a solvent (Figure 3.2). The mixture was then sonicated for about 1 hour at room temperature. The solution was then put in the oven for 24 hours at 80°C to remove the excess solvent. Subsequently, samples were calcined under the N₂ stream at 500°C for 5 hours. The obtained powders were washed several times via centrifugation with ethanol to remove impurities and put in the desiccator.

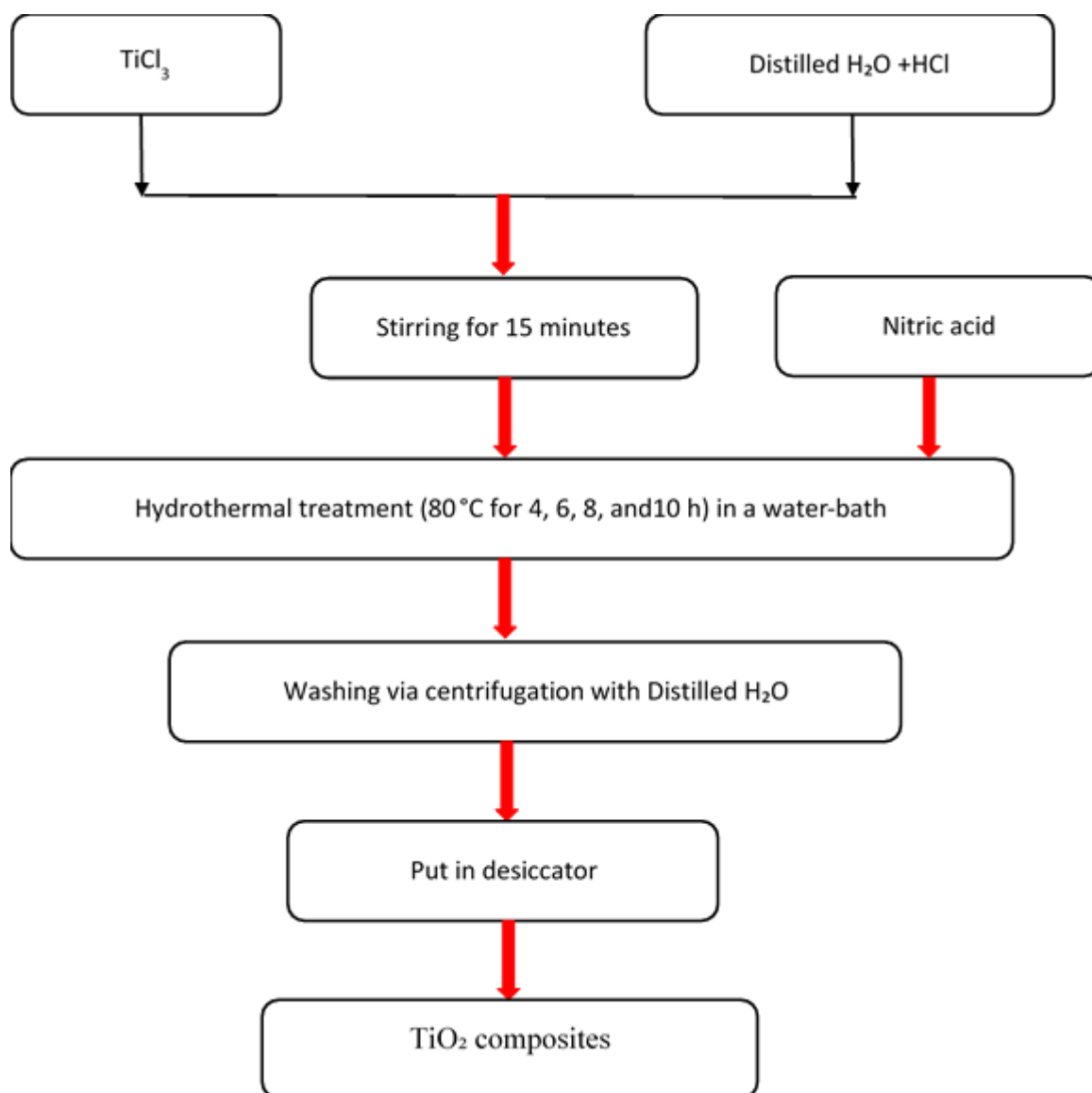


Figure 3.1: Flow chart of synthesis of TiO₂ composites by hydrothermal process.

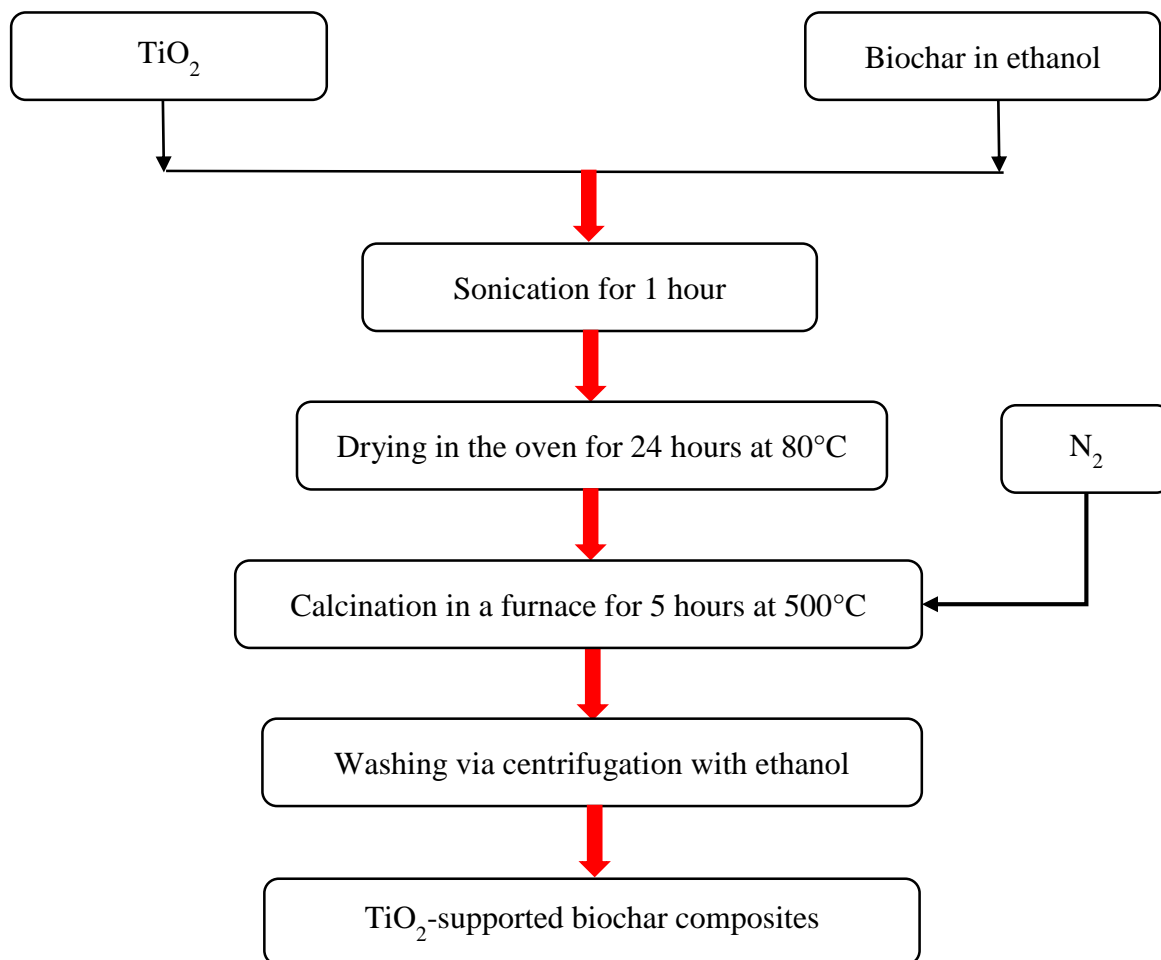


Figure 3.2: Flow chart of synthesis of TiO_2 -supported biochar composites by ultrasound process.

3.2.3. Preparation of simulated textile wastewater

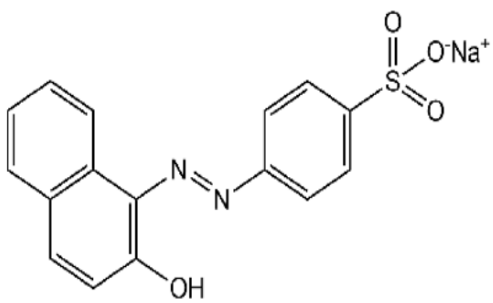
The simulated textile wastewater was prepared by dissolving 20 mg of reactive orange II sodium salt in deionised water in 1000 ml volumetric flasks to obtain a solution of 20 ppm of orange II sodium dye. This solution was sealed in the reagent bottle and stored at room temperature.

3.2.4. Properties of orange II sodium dye

Orange II sodium; also known as acid orange 7, acid orange A and orange II; is an azo dye pH indicator and is relevant in biological applications. Orange II is commonly found in cleaning

products, cosmetics, personal care, food, and beverages. The general characteristics of orange II sodium are summarized in Table 3.1. In this study, orange II was used as a model dye.

Table 3.1: Characteristics data of orange II sodium

Dye structure	Properties
	<ul style="list-style-type: none"> ➤ IUPAC Name: 4-(2-Hydroxy-1-naphthylazo) benzenesulfonic acid sodium salt ➤ Wavelength: 483 nm ➤ Dye class: azo dye ➤ MW: 350.32 g.mol⁻¹ ➤ Molecular formula: C₁₆H₁₁N₂NaO₄S

3.3. PHOTOCATALYTIC DEGRADATION OF ORANGE II SODIUM DYE

The photo-activity of the TiO₂-supported biochar composites was assessed by the photochemical degradation of reactive orange II sodium in simulated textile wastewater under visible light. The investigations were executed in 100 ml of the Teflon container, at room temperature in the presence of air and a constant agitation speed (200 rpm). The TiO₂-supported biochar was spread in a solution of 50 ml of orange II sodium salt (20 ppm). The solution was put in the dark for 20 minutes to set up the adsorption-desorption equilibrium between the TiO₂-supported biochar composites and the reactive orange II sodium molecules. The samples were then put below a 160 W Mega-Ray irradiation lamps light using a UV filter (450 nm) at room temperature in the presence of air and a regular agitation speed (200 rpm). The samples were centrifuged and then monitor via the UV-Visible spectrophotometer to measure dye concentration.

Calculation of photocatalytic efficiency was done on the formula:

$$removal (\%) = 100 \times \frac{C_0 - C}{C_0} \quad (3.3)$$

C_o is the initial concentration of orange II sodium, C is the concentration of orange II sodium when the reaction time is t .

3.4. ANALYSING TECHNIQUES

3.4.1. Ultraviolet-Visible spectrophotometry (UV-VIS)

The Optical properties of the TiO_2 and the TiO_2 -supported biochar composites were measured on a UV-1800 Shimadzu spectrophotometer. The degradation of the orange II sodium dye was also monitored similarly. Measurements were made by putting water (the blank) in the reference cell and the liquid sample in quartz cuvette, the wavelength ranged from 200 nm to 800 nm. The energy band gap of TiO_2 and TiO_2 -supported biochar composites have been obtained by the use of the Tauc method that is expressed with the aid of the following equation (Makula *et al.*, 2018):

$$(\alpha h\nu)^2 = K(h\nu - E_g) \quad (3.4)$$

Where h is the Planck constant, ν is the photon's frequency, α is the molar extinction coefficient, E_g is the band gap energy, K is a constant, and $h\nu$ is the energy of the incident wave.

$$E_g = \frac{1240}{\lambda} \quad (3.5)$$

Where λ is the frequency

$$\alpha = 2.303 \times \log \frac{A}{t} \quad (3.6)$$

Where A is absorbance and t is the thickness of the cuvette.

3.4.2. Fourier transform infrared spectroscopy (FTIR)

The surface performance of the Port Jackson willow leaves, biochar, TiO_2 , and TiO_2 -supported-biochar was characterised with the aid of FTIR. Measurements were made on a Perkin Elmer

1000 series Fourier Transform Infrared (FTIR) spectrometer. The functional groups of the sample were determined through FTIR based on its special absorption frequency. The wave energies are immediately proportional to the absorption frequency given by using Hooke's law:

$$\bar{\nu} = \frac{1}{2\pi c} \sqrt{\frac{k}{\mu}} \quad (3.7)$$

Where $\bar{\nu}$, c , k , and μ are vibrational frequency, speed of light, force/spring constant, and reduced mass of bonding atoms, respectively (Berthomieu & Hienerwadel, 2009).

3.4.3. Scanning Electron Microscopy-Energy Dispersive Spectroscopy (SEM-EDS)

Scanning electron microscopy joined together with energy-dispersive x-ray spectroscopy (SEM-EDS) was used to learn about the surface morphology of Port Jackson willow leaves, Biochar, and TiO₂-supported biochar composites. SEM is the best technique to use because it offers details on the diameter and association of the pores of the sample structure. The SEM instrument used was coupled with EDS to a computerized image investigation system using a backscattered electron beam (BSE). The x-ray detector of the EDS calculates the wide variety of emitted x-rays in opposition to their energy. A spectrum of energy x-rays was obtained and assessed for qualitative and quantitative identification of existing chemical elements in the samples. The powder samples were coated with K950X EMITECH sputter coater for 3 minutes before the analysis. SEM images were obtained using the 1450 Scanning Electron Microscopy Unit at University of the Western Cape.

3.4.4. X-ray diffraction (XRD)

TiO₂ and TiO₂-supported biochar composites have been characterised by XRD to determine their crystal structure and inside atoms arrangement (Bunaciu *et al.*, 2015). XRD spectra were got from a BRUKER AXS D8 Advance x-ray diffractometer outfitted with a LynxEye detector, the use of Cu-K α radiation ($\lambda_{K\alpha 1}=1.5406 \text{ \AA}$) supply in the vary of 5° to 90°. The particle size, D , of the nanomaterial was decided from powder x-ray diffraction (XRD) spectra by using Scherrer's formula:

$$D = \frac{K \lambda}{FWHM \cos\theta} \quad (3.8)$$

The K factor in Scherrer's formula is dimensionless and accounts for the form of the specimen and frequently has the value of 0.9 or close to unity. λ is the wavelength and FWHM is the full width of the peak at half the maximum depth after subtraction of instrumental noise and its represented the diffraction angle in radians, θ is the height position in radians (Jensen *et al.*, 2006).

3.4.5. Brunauer–Emmett–Teller (BET)

The change of the TiO₂ with biochar was studied by using BET. This method uses a size of the physisorption of gas to derive a value of surface area regarding the characterization of porous and finely-dispersed solids for a sample. The gas molecules can skip between particles and into all pores, cracks, and floor roughness so that the measurement probes the full microscopic surface place of the sample. The BET model gives the quantity of adsorption, at a constant temperature, relative to the quantity in a single monolayer. It is a sorption isotherm model (Ambroz *et al.*, 2018):

$$\frac{n_{adsorbed}}{n_m} = \frac{C (P/P_0)}{(1 - P/P_0)(1 + (C - 1)P/P_0)} \quad (3.9)$$

where P and P_0 are the equilibrium and the saturation pressure of adsorbates at the temperature of adsorption, respectively, C is a constant considered to relate the adsorption strength of the first layer to the enthalpy of vaporisation of the liquid adsorbate.

3.5. PARAMETERS AFFECTING THE PHOTOCATALYTIC DEGRADATION PROCESS

3.5.1. Effect of catalyst loading

The catalyst loading is one of the important parameters in the photocatalytic degradation efficiency due to the increase in the quantity of catalyst the number of active sites onto the surface of the catalyst which subsequently leads to the increase of hydroxyl radical (Akpan & Hameed, 2009; Gnanaprakasam *et al.*, 2015). The photocatalytic effectivity of TiO₂ and TiO₂-supported

biochar on the decolouration of orange II Sodium was evaluated at exclusive catalyst loading in the range of 50 mg/L to 250 mg/L for 60 minutes the use of 20 ppm of orange II sodium dye.

3.5.2. Effect of pH

The solution pH affects photocatalytic decolouration because it changes the quantity onto the surface of the catalyst (Ajmal *et al.*, 2014). Hence pH takes an essential part in the qualities of the wastewater and in the dye degradation process during generation of hydroxyl radicals (Riaz, 2013). To study the impact of pH, the degradation of orange II sodium was performed at pH 4 to pH 10 using a solution of 20 ppm of orange II sodium dye. Concentrated sodium hydroxide (NaOH) and concentrated hydrochloric acid (HCl) were used to adjust the pH in the solution.

3.5.3. Effect of initial dye concentration

The initial concentration of organic dyes strongly influences the photocatalytic degradation efficiency and the quantity of dyes adsorbed onto the surface of the catalyst (Chiu *et al.*, 2019). The impact of dye on photocatalytic degradation of orange II sodium was studied in the presence of TiO₂ and TiO₂-supported biochar composites. The initial concentration of dye was varied from 20 ppm to 50 ppm at catalyst loading 200 mg/L.

3.5.4. Kinetics studies

During the photodegradation process, the concentration of orange II sodium dye decreased as a function of time. Therefore, the kinetics of the study was analysed by using the Langmuir-Hinshelwood kinetic model. The pseudo-first-order kinetics were tested for the photodegradation procedure the use of the following equation (3.10):

$$\ln \frac{C_o}{C_t} = Kt \quad (3.10)$$

Where C_o , and C_t represent the initial concentrations of orange II sodium dye, the concentration of orange II sodium dye at time t respectively. K observed pseudo-first-rate coefficient rate

coefficient (Irani *et al.*, 2016). The effect of dye concentration on the rate r of degradation is given in the form of the following equations (3.10):

$$r = \frac{KKC}{1+KC} \quad (3.11)$$

$$\frac{1}{r} = \frac{1}{KKC} + \frac{1}{K} \quad (3.12)$$

where C is the concentration of the orange II sodium dye at time t , K is the reaction rate constant in min^{-1} and K is the Langmuir adsorption constant. K reflects the limiting rate of the reaction at maximum coverage under the given experimental conditions K represents the equilibrium constant for the adsorption of orange II sodium on the illuminated catalyst (Jamil *et al.*, 2012).

3.5.5. Determination of the electrical Energy Efficiency per order (EE_o)

Photocatalytic degradation is an energy process as it uses electrical power for the procedure to run and can affect the running costs. The International Union of Pure and Applied Chemistry (IUPAC) introduced two figures-of-merit for Advanced Oxidation Processes (AOPs) on the utilization of electrical energy (Bolton *et al.*, 2001). In the degradation of low pollutant concentrations, the applicable figure-of-merit is the electrical energy per order (EE_o), described as the number of kilowatt-hours of electrical energy needed to remove 90 % of the pollutant in 1 m^3 of wastewater. The EE_o for the pseudo-first-order was calculated using the following equations (3.13) and (3.14) below:

$$EE_o = \frac{P \times t \times 100}{V_o \times 60 \times \log C_o/C} \quad (3.13)$$

$$EE_o = \frac{P \times 38,4}{V_o \times k} \quad (3.14)$$

Where P is the power (kW) of the system, t (h) is the duration, V_o (m^3) is the treated volume, and C_o and C are the initial and final dye concentrations (mg/L), respectively.

3.5.6. Reusability of the photocatalyst

The reusability of photocatalyst is a very vital key in green technology for an environmental benefit that determines the stability of a photocatalyst (Saggiaro *et al.*, 2011). To evaluate the reusability of TiO₂-supported biochar, the photocatalyst was separated from the reaction combinations by centrifugation, washed numerous times with distilled water and kept in the oven overnight at 80°C and reused for the degradation of orange II sodium under the same conditions for three times.

CHAPTER 4

CHARACTERISATION OF THE BIOCHAR, TiO₂ AND TiO₂-SUPPORTED BIOCHAR COMPOSITES

This chapter discusses in detail the characterisation of the synthesised biochar from *Acacia saligna* (PJW) leaves, TiO₂ from TiCl₃, and TiO₂-supported biochar composites from the mixing of synthesised TiO₂ and biochar. The discussion includes the optical absorption properties of the samples with UV-Vis spectrophotometer and the analysis of the morphology and amorphous structure with scanning electron microscopy (SEM). The functional group identification was done with the aid of Fourier transform infrared spectrophotometry (FTIR). Furthermore, the discussion on structural properties of a sample with XRD and surface area and pore size distribution with Brunauer-Emmett-Teller (BET) were used for further characterization of the synthesized samples.

4.1. CHARACTERISATION OF BIOCHAR OBTAINED FROM PJW LEAVES

The yield of the biochar was obtained after the carbonization of the PJW leaves in the oven. As shown in Table 4.1, the yield increased with the increasing time of pyrolysis from 68.90 % at 1 hour to 70.90 % at 2 hours and then decreased to 70.68 % after 3 hours. Previous studies show that the yield decline due to the combustion of organic materials and the destruction of components such as hemicellulose which decomposes at 220° - 300°C. This process is corresponding to the torrefaction process (Yang *et al.*, 2004; Batista & Gomes, 2021). The chemical composition of the biochar was obtained using EDS analysis. These results revealed the presence of carbon and oxygen as the main constituents and inorganic minerals such as Ca, K, Cl, and S, which could explain the high percentage of the ash content as shown in Table 4.1 below.

The percentage ash content is given in Table 4.2. The results show that the ash content is lower in Port Jackson Willow than in the biochar due to the mineral elements found in the ash remaining in biochar following carbonization (Al-Wabel *et al.*, 2013).

Table 4.1: Yield and chemical compositions of the biochar after varying pyrolysis times.
[PJW leaves weight = 10.0 g; temperature = 285°C].

Pyrolysis Time (hours)	Yield (%)	Carbon (%)	Oxygen (%)	Others elements (%)
1	68.90	78.62	19.05	2.33
2	70.90	75.11	22.26	2.63
3	70.58	77.57	19.30	3.14

According to Stella et al. (2016), the carbonaceous material is divided according to the percentage of the ash content such as low (< 5 %), medium (5 – 10 %), and high (> 10 %). Therefore, the ash content of PJW leave of 8.07 % was medium, and the ash content of biochar was classified as high.

Table 4.2: Ash content at different times

Sample	Pyrolysis time (hours)	Ash content (%)
Port Jackson Willow	-	8.07
Biochar	1	10.55
Biochar	2	10.76
Biochar	3	11.23

The Fourier transform infrared spectra of the PJW leaves and the biochar prepared at different times are similar and are shown in Figure 4.1. The band at 3261 cm^{-1} is attributed to the -OH stretching vibration due to the surface adsorbed moisture. The peaks at 2991 and 2847 cm^{-1} are assigned to -CH₂- symmetric stretching of an alkyl which is consistent with the C-H stretching appearing at 1376 cm^{-1} (Saraswati *et al.*, 2015). The peaks 1721 and 1446 cm^{-1} are attributed to the C=O stretching vibration in the carboxylic groups. The 1629 cm^{-1} is ascribed to the C=C stretching variation in aromatic rings (Tahir, 2019). The absorption peaks at 1039 cm^{-1} correspond and to the C-O-C stretching vibration from esters and ethers (Maulidiyah *et al.*, 2015; Gee *et al.*, 2020). The small peak at 832 cm^{-1} proves the presence of an alkene out-of-plane bend. The band below 1000 cm^{-1} shows the presence of a metal oxide mode which indicates the presence of a metal, as also supported by EDS analysis (see Section 4.5).

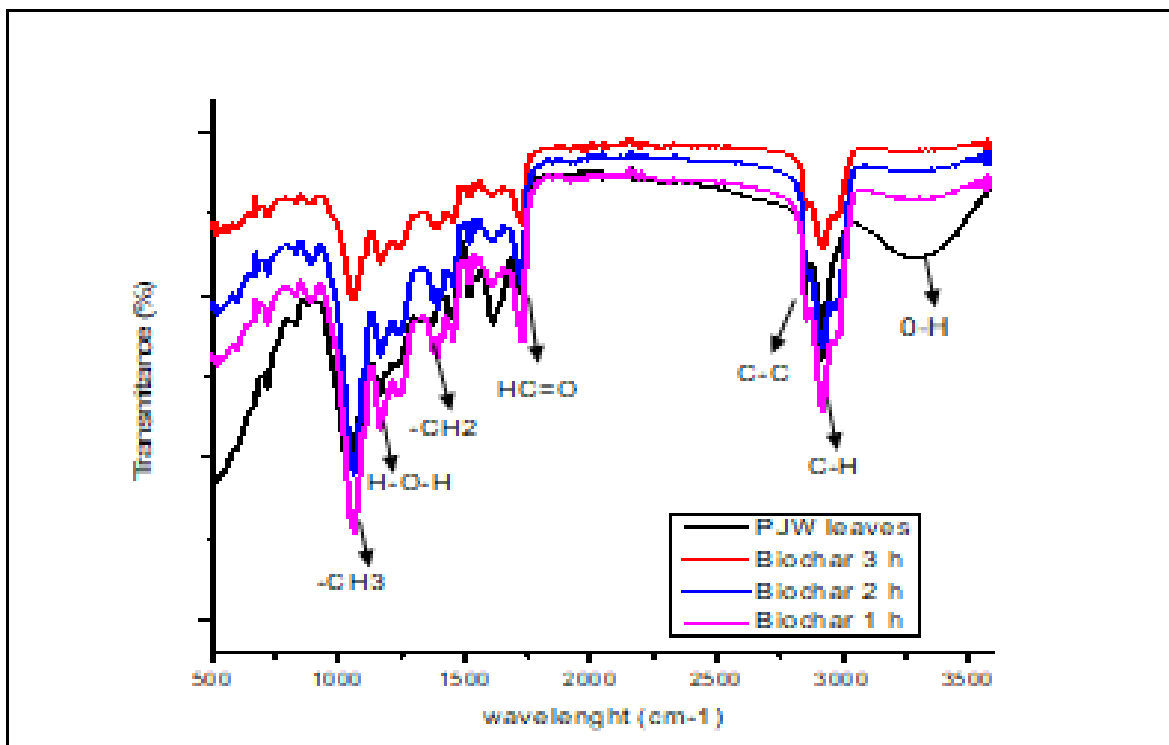


Figure 4.1: FTIR spectra of PJW leaves and Biochars at 1 h, 2 h, and 3 h.

Figure 4.2 gives the SEM images of the surface morphology of the PJW and synthesized biochars. These appear rough and display a morphology with irregular and small porous surfaces that indicated a low porosity.

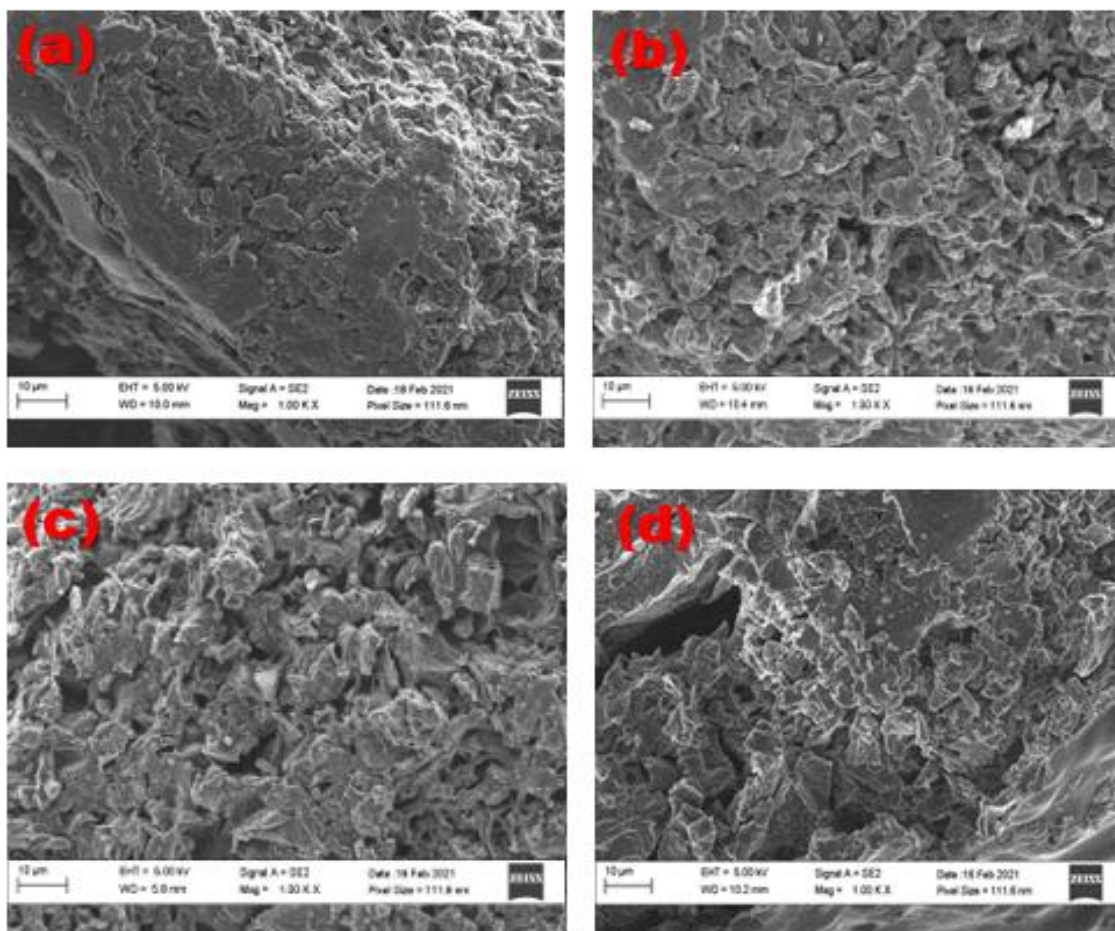


Figure 4.2: SEM images 10 µm: (A) Port Jackson Willow leaves (B) biochar at 1 h (C) biochar at 2 h and (D) biochar at 3 h.

X-ray scattering revealed structural similarity among the biochars at 2 h and 3 h, which can make them more resistive in the environment, heavily depending on their physical structure. The peak was at 15° , which was assigned to the completely ordered regions of cellulose. The extended signals centred at 23° and 43° in the biochar diffractogram confirmed the presence of amorphous carbon; the signal at 51° that indicated the presence of carbon nanofiber according to the JCPDS database (Singh *et al.*, 2016; Xing *et al.*, 2016). The X-ray diffraction patterns of PJW leaves and biochars prepared at different times are provided in Figure 4.3 below.

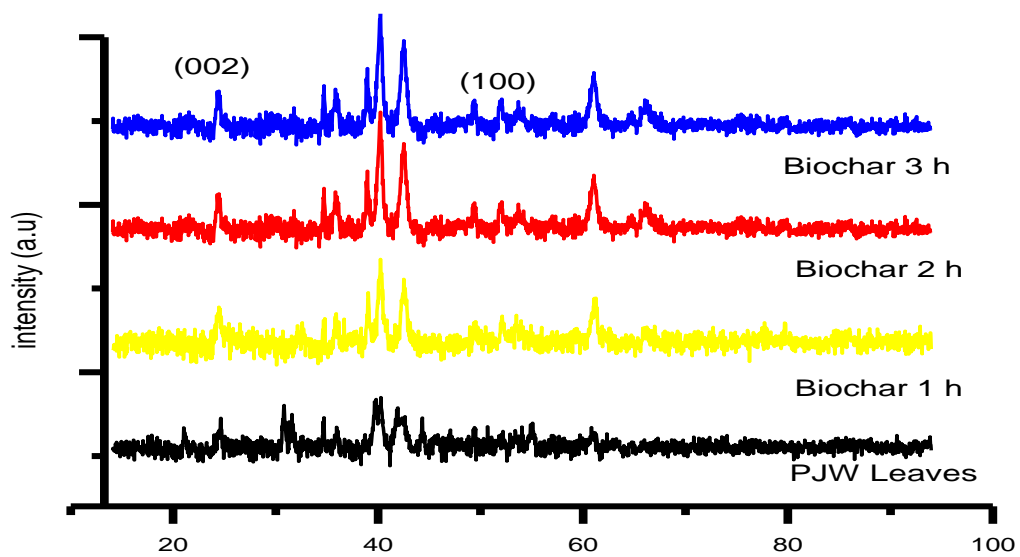


Figure 4.3: XRD pattern of PJW leaves and biochar prepared at 1 h, 2 h, and 3 h.

4.2. UV-VISIBLE SPECTROSCOPY OF THE SYNTHESISED TiO₂-SUPPORTED BIOCHAR

As shown in Figure 4.4 (a), a small absorption below 400 nm on the spectra of TiO₂ demonstrates the rutile TiO₂ phase which was confirmed on the XRD (Zhang *et al.*, 2010). Compared to the spectrum of TiO₂, a small absorption above 400 nm in the spectrum of the TiO₂-supported biochar composite shows a contribution of the biochar on the TiO₂ and is shown in Figure 4.4(b) indicating that the TiO₂-supported biochar might have a higher photocatalytic activity under visible light irradiation. Similar observations are reported by Park *et al.* (2005) and Zhang *et al.* (2011).

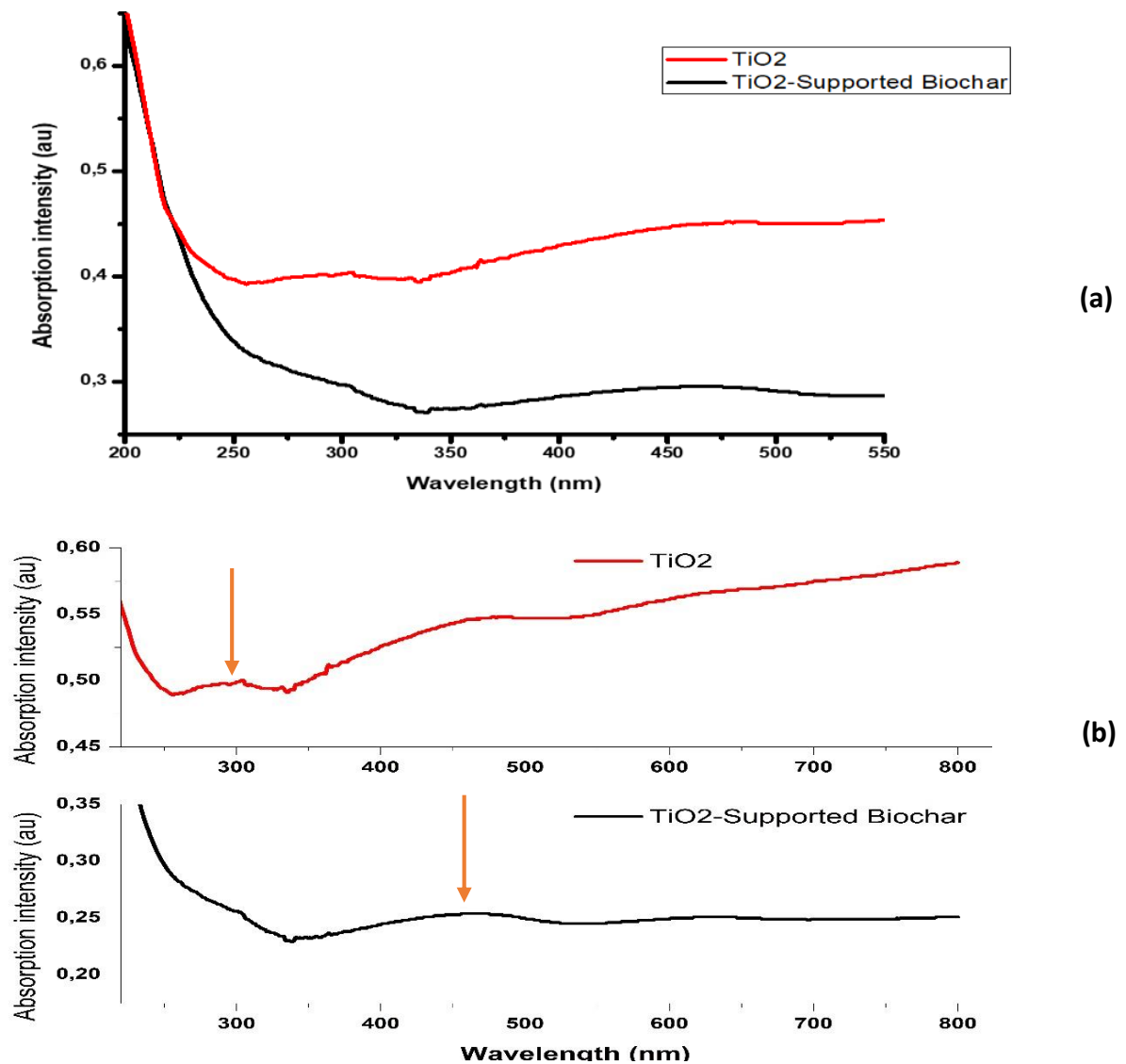


Figure 4.4: UV-Visible spectra range from (a) 200–550 nm and (b) 300–800 nm for TiO₂ and TiO₂-supported biochar composites.

4.3. DETERMINATION OF ENERGY BAND GAP TiO₂-SUPPORTED BIOCHAR

The energy band gap of TiO₂ and TiO₂-supported biochar composites were measured with a UV-Vis spectrophotometer using the Tauc method. Figure 4.5 shows the Tauc plots of (a) TiO₂ and (b) TiO₂-supported biochar nanocomposites synthesised.

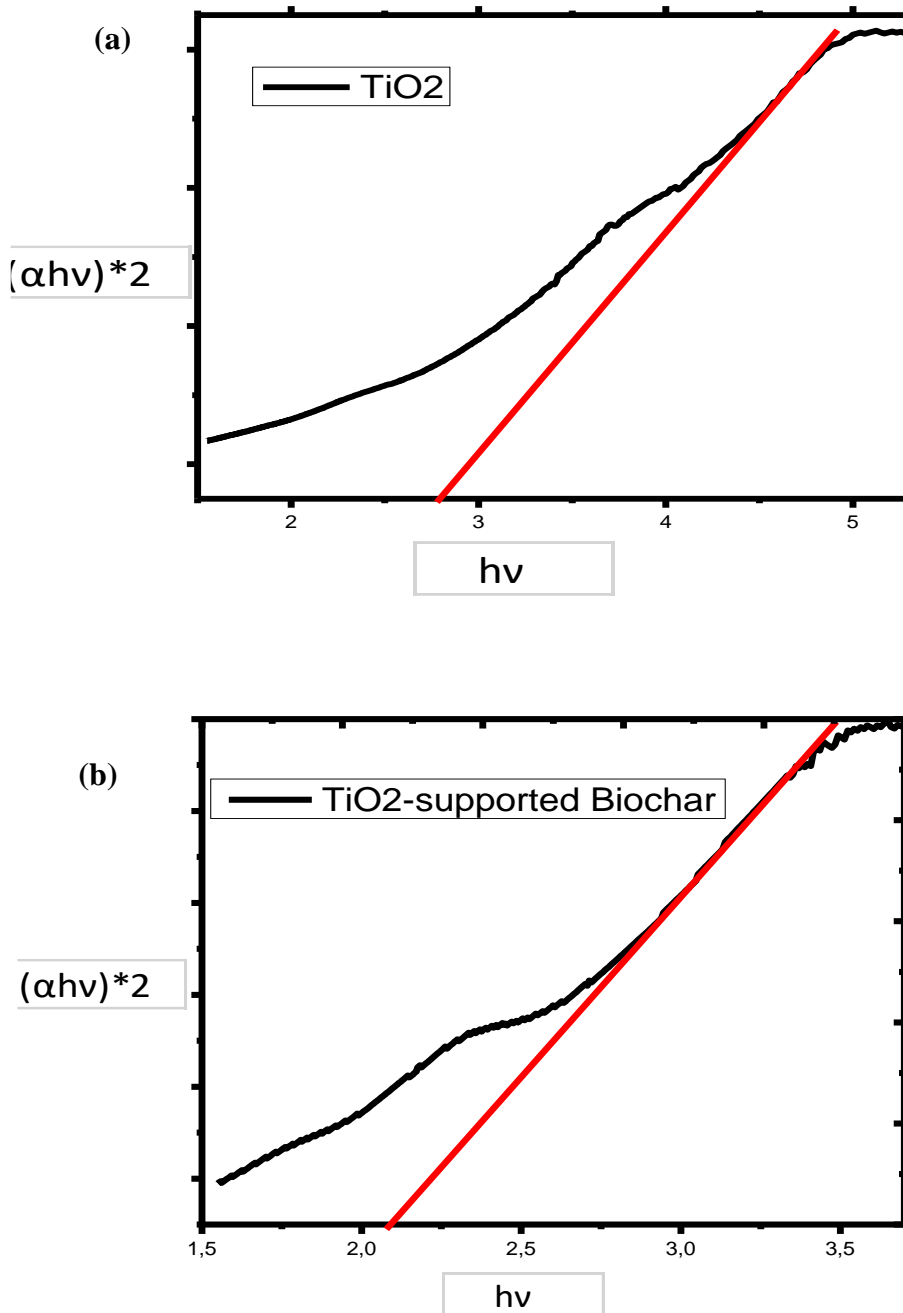


Figure 4.5: Energy band gap (Tauc plots) (a) TiO₂ and (b) TiO₂-supported biochar composites.

The energy band gap of the synthesised TiO₂ composite was determined to be 2.81 eV. According to Radha *et al.* (2018), this band gap is due to the formation of rutile TiO₂ which has a lower band gap and can be confirmed with XRD. Compared with TiO₂, the energy band gap of TiO₂-supported biochar composite was measured to be 2.11 eV, and the absorption range of the photocatalyst is more expanded to the visible spectrum. TiO₂ is grown on the in-situ biochar-supported by Ti-O-C bond, and the carbon 2*p* and oxygen 2*p* atomic orbitals are hybridized under 500°C in the presence of gas after nitrogen causing the formation of sub-band levels between the

VB and CB. This leads to an increase in the edge of the valence band, which reduces the band gap (Liu *et al.* 2019). This result indicates that the modification of TiO₂ with biochar reduces the energy band gap by about 0.7 eV, expanding it into the visible light region. Therefore, the TiO₂-supported biochar composite shows greater promise as a solar active photocatalyst than the TiO₂ synthesised. It has been reported by Chao *et al.* (2009), Hu *et al.* (2013), Wei *et al.* (2014), Syafei *et al.* (2017), Sarunas *et al.* (2019), Cheol *et al.* (2021) and Au-pree *et al.* (2021) that doping TiO₂ with a carboneous material produce a composite with an energy band gap from 2.2 to 3.2 eV. The band gap of 2.11 eV for the TiO₂-supported biochar prepared in this study is lower than the band gaps reported by the authors above.

4.4. FTIR ANALYSIS

The Fourier transform infrared (FTIR) characterization of synthesised nanocomposites is shown in Figure 4.6. The spectra of TiO₂ show a band around 3003 cm⁻¹ corresponding to stretching and a peak 1647 cm⁻¹ corresponding to bending vibration of a hydroxyl group (OH) representing the water (H-O-H) as moisture. The 1045 - 1056 cm⁻¹ attributed to the Ti-O stretching which is the characteristic peak of TiO₂. The stretching mode of the hydroxyl (O-H) group in water as moisture is not visible in TiO₂-supported biochar spectra due to the high temperature used during the synthesis (Singh *et al.*, 2016; Zhang *et al.*, 2017).

The FTIR-spectra of TiO₂-supported biochar shows two absorption peaks around 3006 cm⁻¹ that demonstrate the C-H stretching mode of the double bonds (=CH) group and 2906 cm⁻¹ corresponding to the C-H asymmetric stretching in aliphatic (C-C) groups, this peak appears with higher intensity in the TiO₂-supported biochar (Saraswati *et al.*, 2015). A peak observed at 1223 cm⁻¹ corresponding to the C-O broad stretch, this bond occurred because of glycosidic linkage of C-O-C and ethanol (Maulidiyah *et al.*, 2015; Gee *et al.*, 2020). The TiO₂-supported biochar spectrum indicates a peak at 1073 cm⁻¹ that suggested the vibration of Ti-O-C coming from the surface attachment of TiO₂ on biochar which is favourable in enhancing the photocatalytic activity of the TiO₂ (Singh *et al.*, 2016).

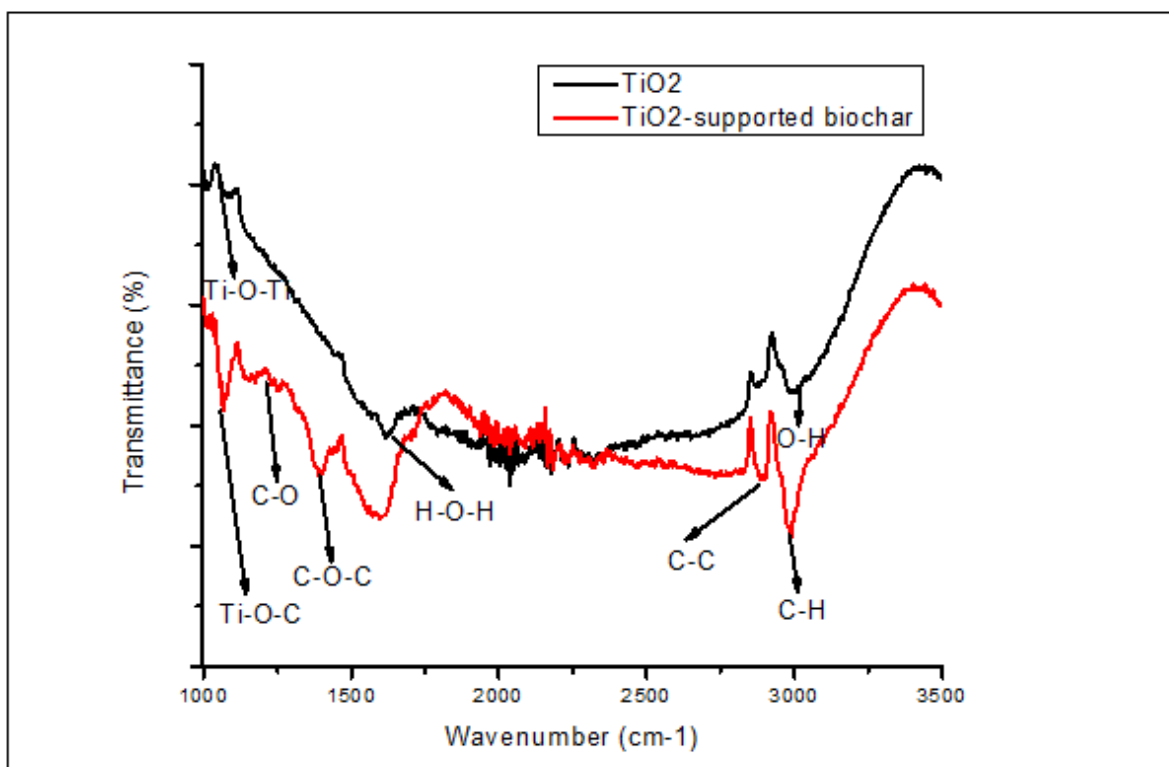


Figure 4.6: IR-spectra of TiO₂ and TiO₂-supported biochar composites.

4.5. SCANNING ELECTRON MICROSCOPY ANALYSIS

The SEM images of the samples and the corresponding EDS are shown in Figure 4.7. The result confirms that TiO₂ was successfully immobilized on the biochar external surface through ultrasound process. TiO₂-supported biochar composite was smooth with a disparate distribution and apparent agglomeration of TiO₂ on the biochar surfaces.

Table 4.3 shows the elemental compositions of TiO₂ and TiO₂-supported biochar based on dispersion efficiencies. The EDS spectrum of TiO₂ shows the presence of O (41.10 %) and Ti (43.45 %) indicating that the nanocomposite is in form of Titanium oxide with C (15.14 %) coming from the coating material during the SEM analysis.

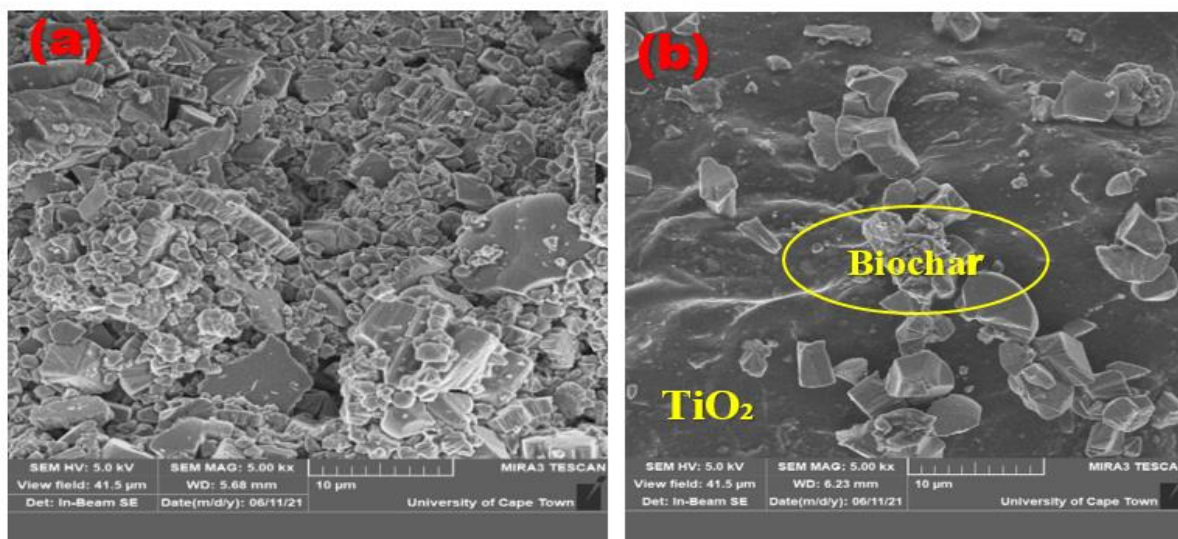


Figure 4.7: SEM images of the (a) TiO_2 and (b) TiO_2 -supported biochar composites.

The EDS spectrum of the TiO_2 -supported biochar shows the presence of C (34.49 %), O (39.71 %), and Ti (24.29 %) as the main elements in the composite suggesting that the TiO_2 -supported biochar was successfully synthesised.

Table 4.3: Chemical composition of the composites.

Elements	TiO_2 (Wt%)	TiO_2 -supported biochar (Wt%)
C	15.14	34.59
O	41.40	39.71
Ti	43.45	24.29
K	-	0.69
Ca	-	0.72
Total	100	100

4.6. BRUNAUER EMMET TELLER SURFACE AREA ANALYSIS

The Brunauer-Emmett-Teller (BET) method was used to determine the surface area and pore size distribution of the photocatalyst. Table 4.4 shows the results of the adsorption/desorption isotherms measurements for TiO_2 and TiO_2 -supported biochar composites with relative pressure

(p/p^0) ranging from 0.011 to 0.999. Figure 4.8 shows N_2 adsorption-desorption isotherms of (a) TiO_2 and (b) TiO_2 supported biochar composites. The curves of TiO_2 and TiO_2 -supported biochar composites exhibited a small hysteresis phenomenon representing a typical type-IV isotherm attributed to mesoporous material with low porosity (Neimark *et al.*, 2008).

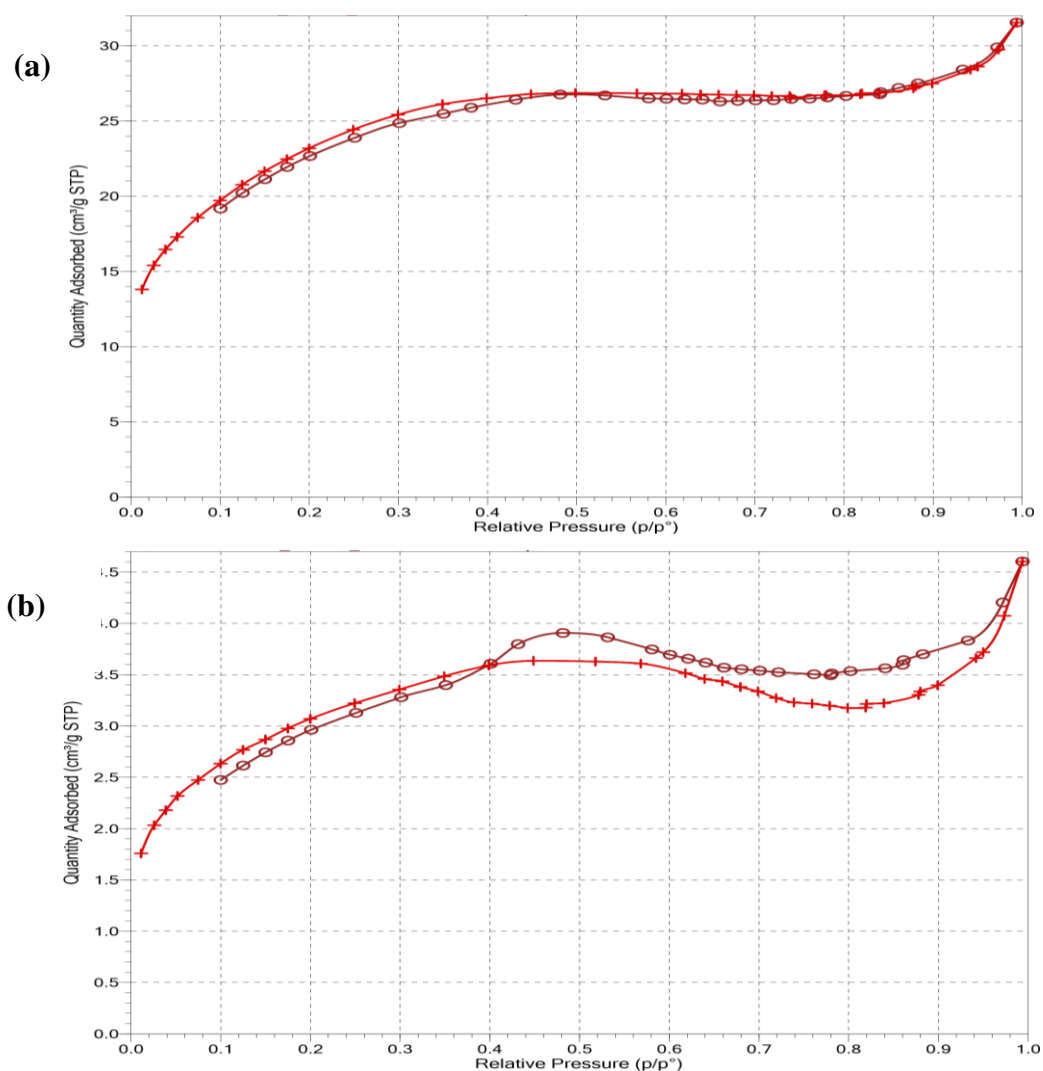


Figure 4.8: N_2 adsorption-desorption isotherm of (a) TiO_2 and (b) TiO_2 -supported biochar composites

The surface area of TiO_2 is $84.45 \text{ m}^2/\text{g}$. After the doping of biochar on the TiO_2 , the surface area was reduced to $11.11 \text{ m}^2/\text{g}$ due to the blockage of carrier pores caused by the loading of biochar and the collapsing of pores walls (Zhang *et al.*, 2017). These results also show that the pore volume of TiO_2 -supported biochar greatly decreases after the deposition of TiO_2 into the biochar surface due to the TiO_2 agglomerations blocking the surface of biochar pores. The higher surface area of TiO_2 was favourable for the growth of adsorption and photocatalytic activity for the pollutant by ensuring a higher contact time.

Table 4.4: The specific surface area and pore structure parameters of TiO₂ and TiO₂-supported biochar composites.

Photocatalyst	Surface Area (m ² /g)	Pore size (Å)	Pore volume (cm ³ /g)
TiO ₂	84.25	10.133	0.0488
TiO ₂ -supported biochar	11.11	9.793	0.0071

4.7. X-RAY DIFFRACTION (XRD) ANALYSIS

The X-ray diffraction patterns of TiO₂ and TiO₂-supported biochar composites are provided in Figure 4.9. According to the JCPDS Card No: 21-1276 as reported by Joni *et al.* (2018), the distinctive peaks at 2θ angles in the TiO₂ composite are corresponding to the TiO₂ rutile phase. The position of 2θ corresponds to Miller indices of (110), (101), (111), (211), (220), (002), and (301) crystalline planes. In the TiO₂-supported biochar, the observed (220), (301), and (200) crystalline planes are clearly a characteristic of TiO₂ anatase. These results reveal the presence of rutile and anatase crystalline phase in the TiO₂-supported biochar, due to the doping of biochar. According to Zhang *et al.* (2017), photocatalysts that contained anatase and rutile phases are more efficient than those with only one crystalline phase.

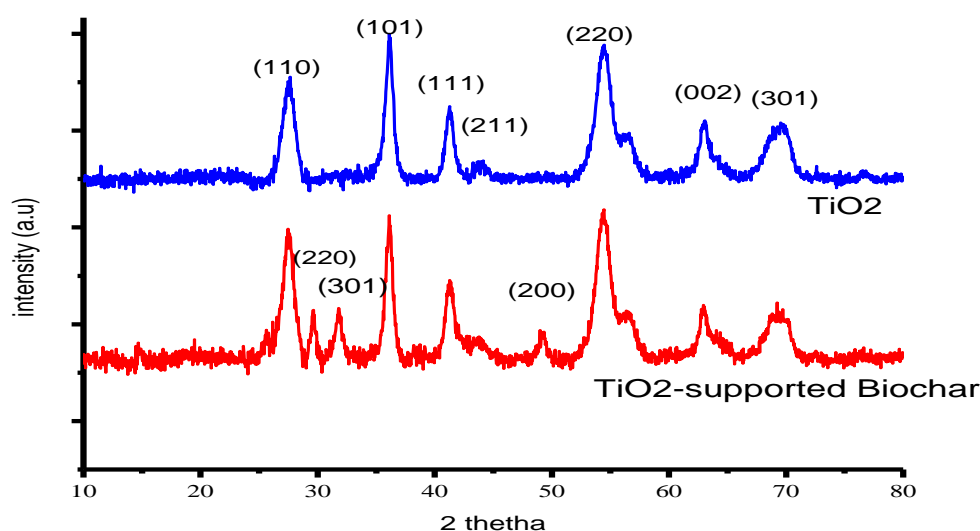


Figure 4.9: XRD patterns of TiO₂ and TiO₂-supported biochar composites.

The strongest peaks of TiO₂ and TiO₂-supported biochar composites, calculated using Equation 3.8 in Section 3.4.4 (Jensen *et al.*, 2006), were shown at 2θ equal to 36.08° and 54.39°, with corresponding crystallite size (d spacing) of 7.158 nm and 7.927 nm, respectively. Table 4.5 gives the values of the crystallite size of the photocatalyst.

Table 4.5: XRD data of TiO₂ and TiO₂-supported biochar composites

Photocatalyst	2θ (The strongest peak)	β (rad)	Crystallite size (nm)
TiO ₂	36.08°	0.01937	7.158
TiO ₂ supported biochar	54.39°	0.01749	7.927

CHAPTER 5

PHOTOCATALYTIC DEGRADATION OF ORANGE II SODIUM DYE

This chapter covers the photocatalytic degradation of reactive orange II sodium dye using TiO₂-supported biochar composite as visible-light-driven nanocomposite. To evaluate the photocatalytic performance of the composite an adsorption study was conducted. Effects of parameters such as catalyst loading, initial concentration of dye, time on removal, and pH were investigated.

5.1. DETERMINATION OF MOLAR EXTINCTION COEFFICIENT OF ORANGE II SODIUM

The molar extinction coefficient is an important factor that serves to establish the quantitative nature of dyes (French, 2009). The absorption spectra of orange II sodium for concentrations ranging from 2 mg/L to 10 mg/L were obtained following the Beer-Lambert law (Mainya *et al.*, 2013). Figure 5.1 shows the Lambert-Beer law plot of the dye at $\lambda_{max} = 483$ nm.

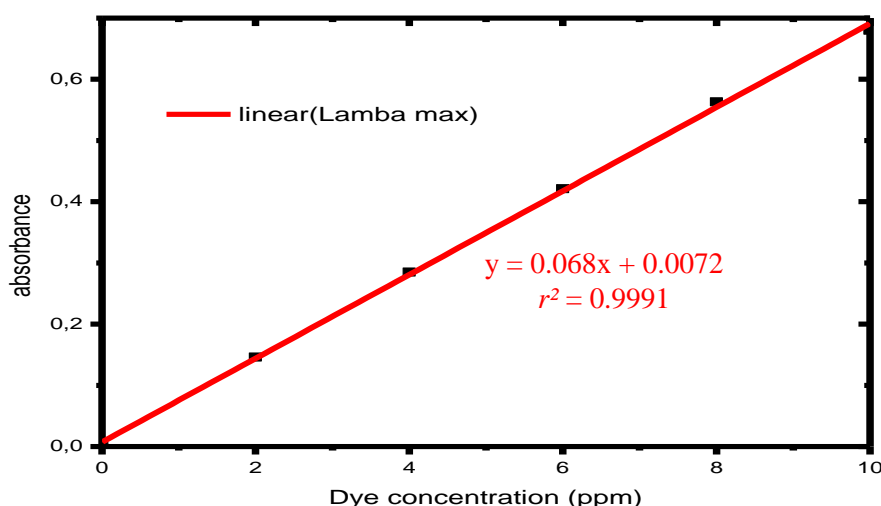


Figure 5.1: Beer's law plot for orange II sodium dye.

As shown in previous studies, the increase of dye concentration generated a proportional increase of absorbance values which indicates that molecular aggregates are not formed in solutions of orange II sodium (Semeraro *et al.*, 2015). Figure 5.2 shows the UV-Visible spectra of orange II sodium dye.

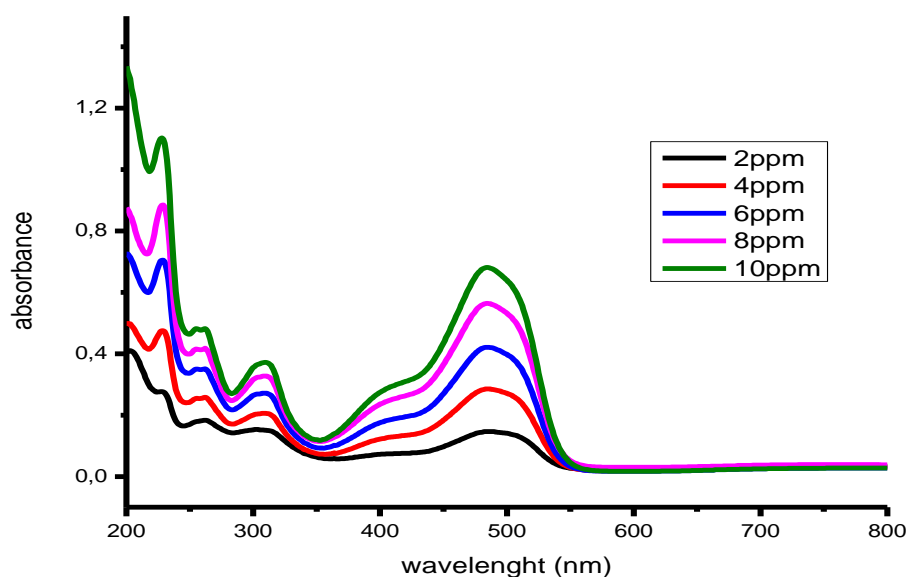


Figure 5.2: UV-Visible spectra of orange II sodium dye

5.2. BATCH STUDY

5.2.1. Effect of catalyst loading

It was observed that increasing the catalyst loading from 50 mg/L to 200 mg/L increased the photocatalytic degradation of orange II sodium from 12.47 % to 12.76 % for TiO₂ and 28.58 % to 55.34 % for TiO₂-supported biochar, respectively as shown in Figure 5.3. The results indicated that the photodegradation efficiency is directly proportional to the catalyst loading. This indicated a true catalytic regime that can be attributed to the increase in photoreactive sites available on the surface of biochar which contributes to the high photocatalytic activity of the nanocomposite (Lin *et al.*, 2013). However, no further increases in efficiency were observed beyond 200 mg/L due to an increase in turbidity and low light penetration of a catalyst (Sintayehu *et al.*, 2017). The photocatalytic degradation was most effective at 200 mg/L catalyst concentration; therefore, all experiments were continued with a 200 mg/L dosage.

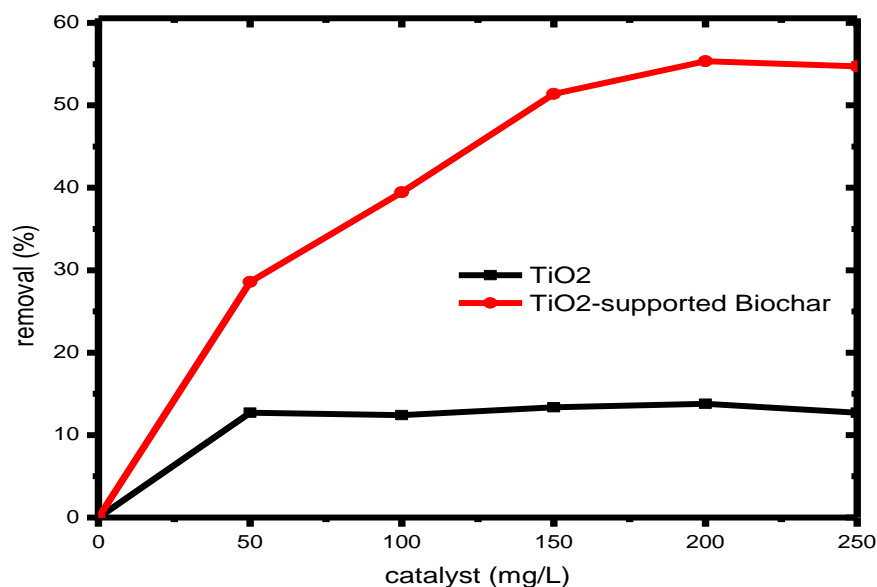


Figure 5.3. Effect of catalyst loading on the photodegradation efficiency of orange II sodium. [C_{dye} =20 ppm, pH = 6.8, time = 60min].

5.2.2. Effect of pH

The results indicate that the photocatalytic efficiency is strongly affected by the pH of the solution as shown in Figures 5.4 and 5.5. The photocatalytic degradation using TiO₂ as photocatalyst was influenced by the pH. At pH 4, enhanced efficiency in the photodegradation of 20.61 % was observed. Increasing the pH from 4 to 10 had a negative effect on the degradation efficiency, resulting in a 13.16 % degradation at pH 10. This suggests that an acidic condition is favourable for the formation of the reactive intermediate hydroxyl radicals (Kumar, 2016). TiO₂ photocatalysts have been reported to exhibit higher oxidizing activity at lower pH (Al-Amin et al., 2016). In contrast, the higher photocatalytic efficiency of orange II sodium using TiO₂-supported biochar was found to be of 83.48 % at pH 6.8 with a minimum of 73.08 % at pH 10. Jamil *et al.* (2012) and Sintayehu *et al.* (2017) reported that a higher photocatalytic efficiency was observed in a neutral medium due to the undissociative nature of the dye which lead to strong adsorption onto the catalyst surface, then a decrease in efficiency was observed due to the negatively charged nature of the photocatalyst surface in a basic medium.

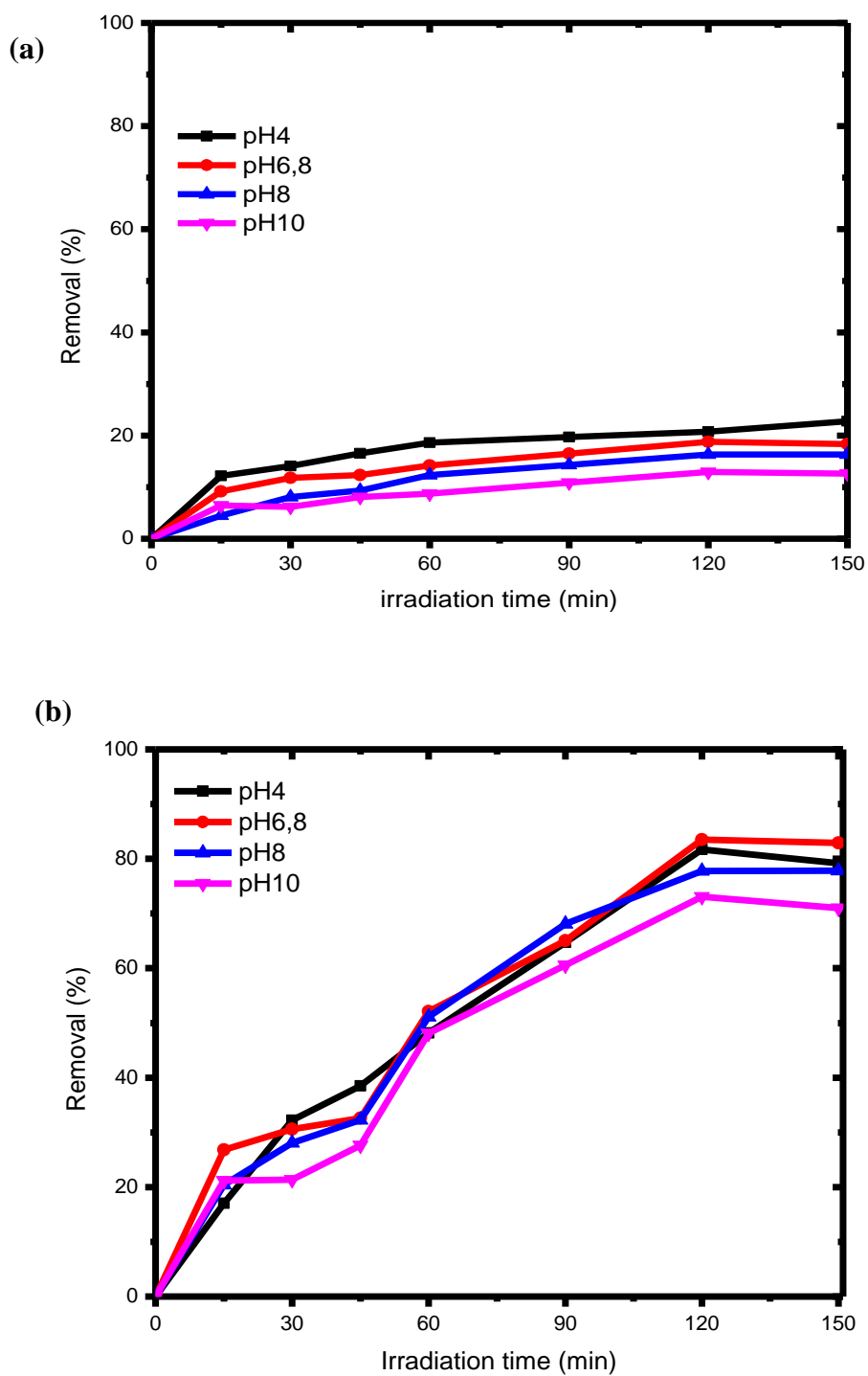


Figure 5.4: Removal efficiency of the effect of pH on orange II sodium decolourisation, and degradation with (a) TiO₂ and (b) TiO₂-supported biochar composites [C_{dye}=20 ppm, C_{cat}= 200mg/L].

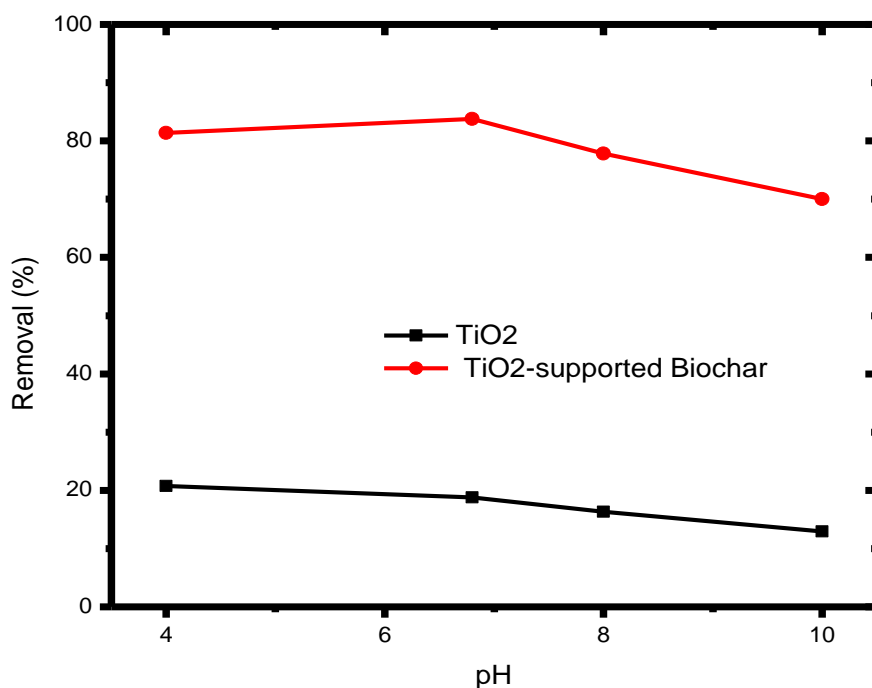


Figure 5.5: Effect of pH on the photodegradation efficiency of orange II sodium.

[C_{dye} =20 ppm, C_{cat}=200 mg/L, time = 60min].

5.2.3. Effect of initial dye concentration

A decrease in the photodegradation efficiency from 18.39 % to 4.42 % for TiO₂ composites and 83.50 % to 60.60 % for TiO₂-supported biochar composites respectively was observed as shown in Figures 5.6 and 5.7. The photodegradation efficiency was inversely affected by the dye concentration due to the equilibrium adsorption of dye on the catalyst surface which results in a decrease in the active sites on the catalyst surface. This phenomenon results in the lower formation of OH^{*} radicals which were considered as the primary oxidizing agents of the organic dye (Madhusudhana *et al.*, 2012).

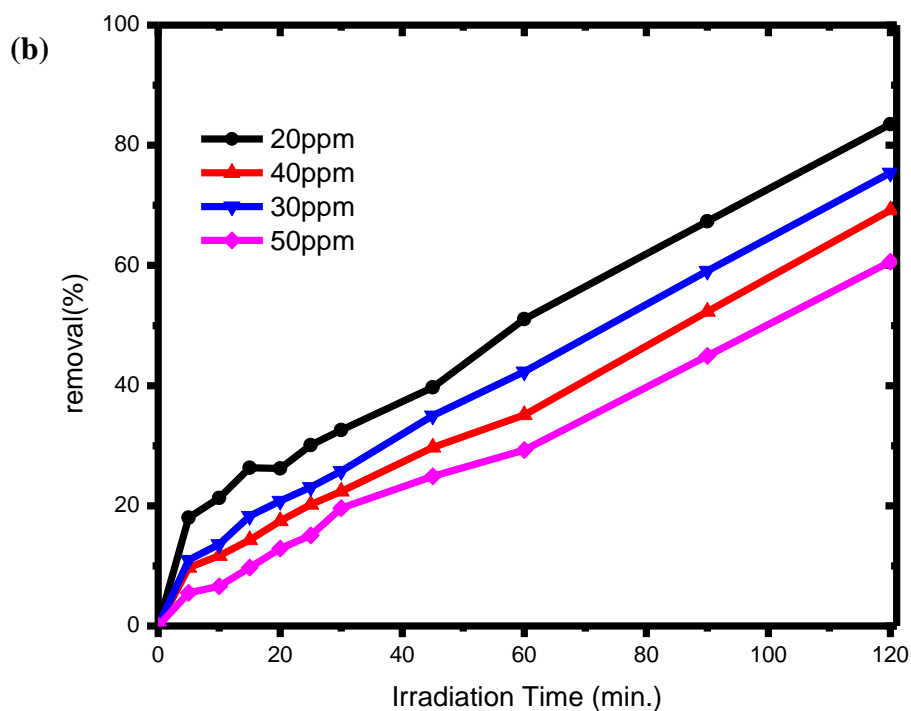
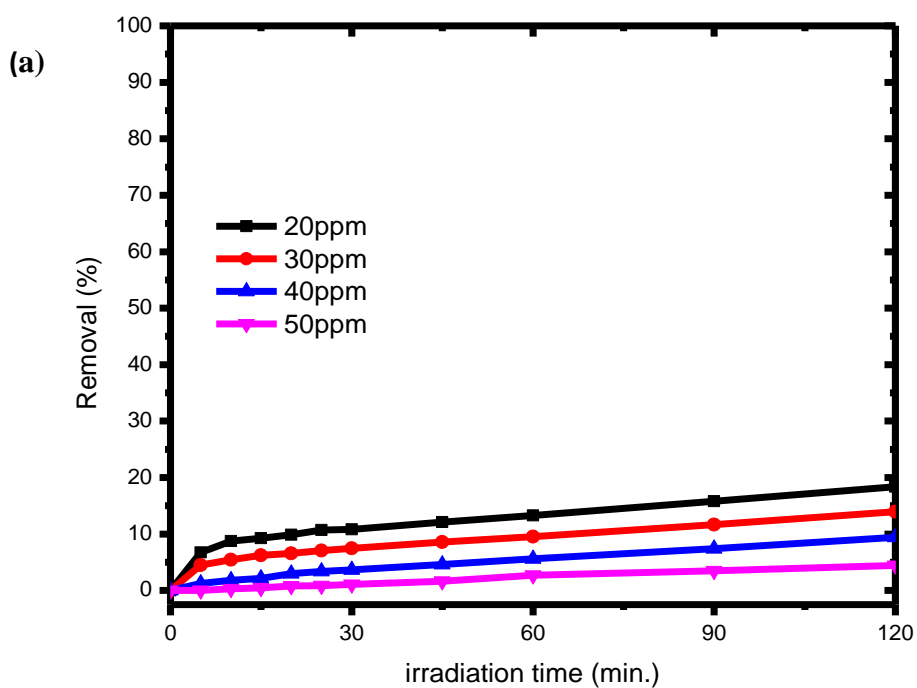


Figure 5.6: Effect of the initial concentration of dye on the photodegradation efficiency of orange II sodium using (a) TiO₂ and (b) TiO₂-supported biochar composites [C_{cat}= 200 mg/L, pH= 6.8].

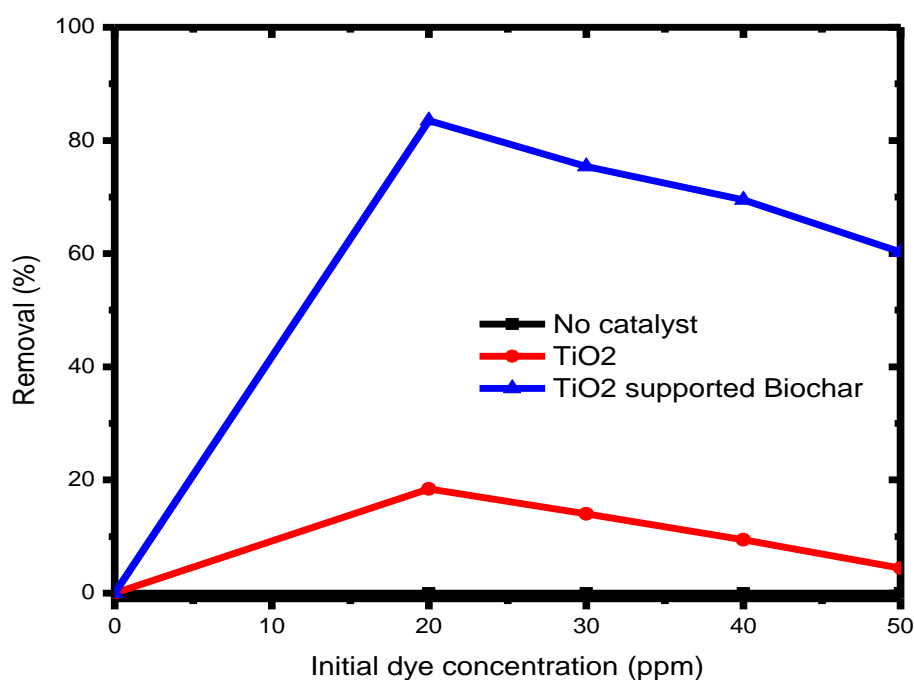


Figure 5.7: Effect of initial dye concentration on the photodegradation efficiency of orange II sodium. [C_{cat} = 200 mg/L, pH = 6.8, time = 60 min].

5.2.4. Kinetics of the photodegradation of orange II sodium dye

The kinetic studies for orange II sodium degradation using both TiO₂ and TiO₂-supported biochar composites were fitted as shown in Figures 5.8. The degradation of orange II sodium by TiO₂ and TiO₂-supported biochar follows the pseudo-first-order and respects the Langmuir-Hinshelwood kinetic model as shown in Table 5.1 below. From this table, the values of the r^2 obtained for TiO₂ and TiO₂-supported biochar composites showed that the photocatalytic degradation process of orange II sodium was suited to be described by the pseudo-first-order model. Jamil *et al.* (2012), Singh *et al.* (2016) and Nguyen *et al.* (2020) reported the same results. The second order kinetics were also fitted, however, the correlation coefficient showed poor correlation for all the samples.

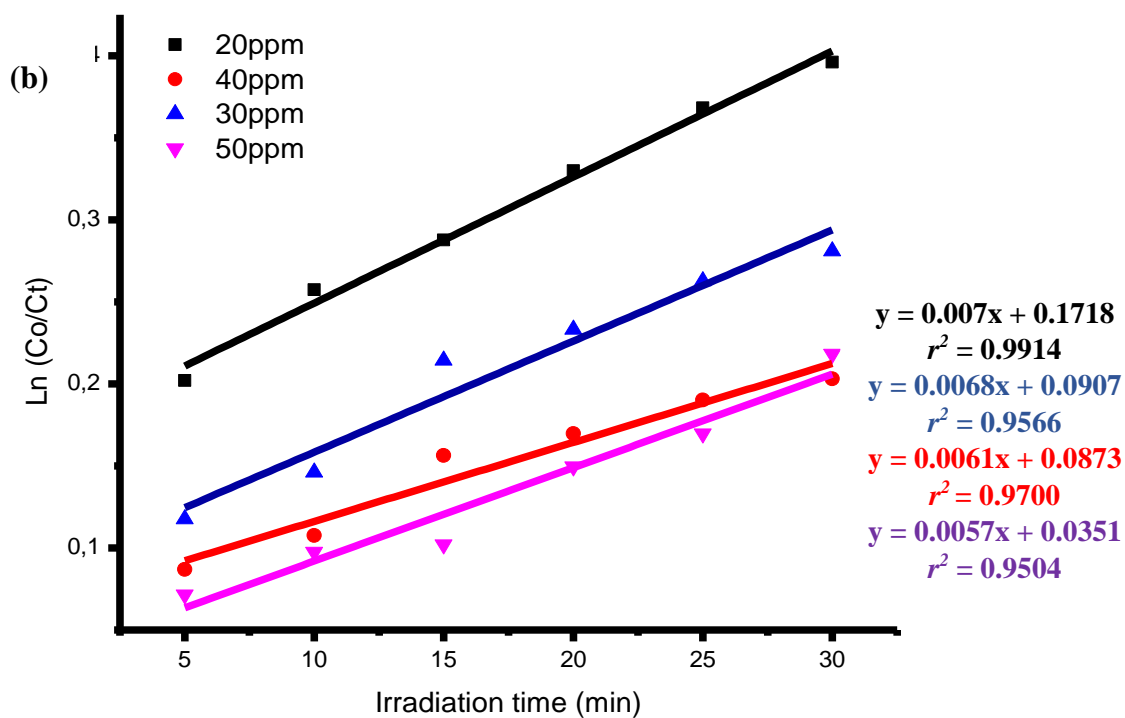
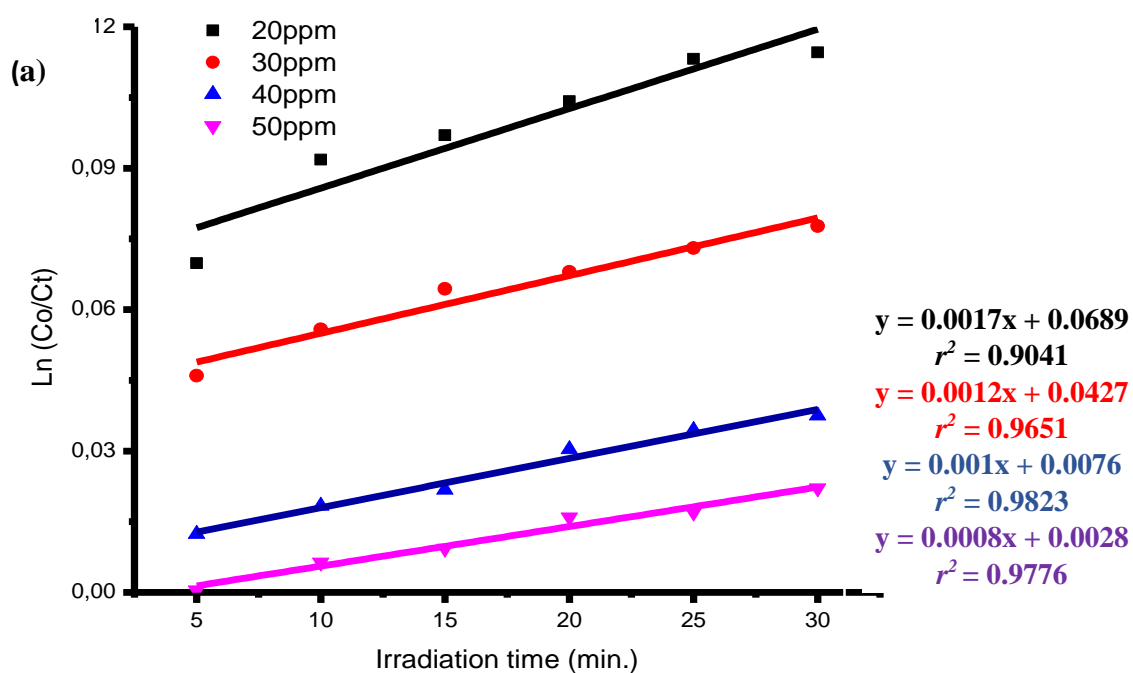


Figure 5.8: Plot of $\text{Ln}(\text{Co}/\text{Ct})$ versus irradiation time in the degradation of orange II sodium dye using (a) TiO_2 and (b) TiO_2 -supported biochar composites
 [Ccat= 200 mg/L, pH= 6.8].

According to Equation 3.11 (in Section 3.5.4), the plot of $1/K$ versus dye concentration is demonstrated in Figure 5.9. The results show a linear variation with a correlation coefficient close to 1, $r^2=0.8404$ for TiO_2 and 0.9621 for TiO_2 -supported biochar respectively, which affirmed that the photocatalytic degradation reaction obeys the Langmuir-Hinshelwood kinetic model. Yetim & Tekin (2016) reported that this result is due to the generating hydroxyl radicals by cavitation without a direct change in the structure of dye. Jadaa *et al.* (2021) also obtained the same results.

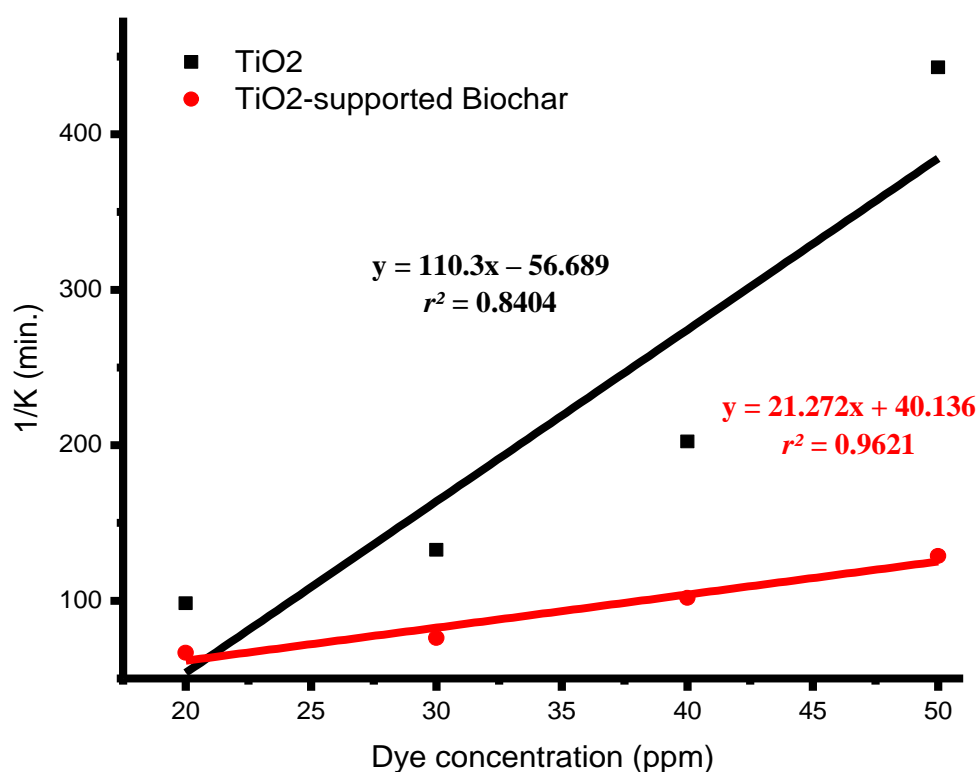


Figure 5.9: Plot of $1/K$ versus dye concentration in the degradation of orange II Sodium dye [Ccat= 200 mg/L, pH= 6.8, time=120 min.].

The values of K of 0.0102 min^{-1} for the 20 ppm dye concentration using TiO_2 composite indicated its lower performance under visible light. The value of K of 0.015 min^{-1} for the 20 ppm dye concentration using TiO_2 -supported biochar composites indicates its good photocatalytic activity which confirms the photo-activity of TiO_2 -supported biochar composites in the visible (Yang *et al.*, 2004). Ayoub *et al.*, 2017 reported that the change in rate is due to the formation of more active site on the photocatalyst during the kinetics process.

Table 5.1: Kinetic parameters of orange II Sodium dye using TiO₂ and TiO₂-supported biochar composites (C_{cat} = 200 mg/L) for 120 minutes at pH 6.8.

Photocatalyst	Dye concentration (ppm)	$k \times 10^{-3}$ (min ⁻¹)	r^2	$1/K$ (min)
TiO ₂	20	10.2	0.9041	98.04
	30	7.5	0.9651	133.33
	40	4.9	0.9823	204.08
	50	2.2	0.9776	454.54
TiO ₂ -supported biochar	20	15	0.9914	66.66
	30	13.2	0.9566	75.75
	40	9.8	0.9700	102.04
	50	7.8	0.9504	128.20

5.2.5. Electrical Energy Efficiency per order (EE_o) of the photocatalytic degradation of orange II sodium dye

The EE_o values for the photodegradation process are given in Table 5.2. The lowest value of EE_o of 136.49 kWh/m³ was obtained using TiO₂-supported biochar at pH 6.8. The results confirm that photocatalytic degradation is affected by the solution pH. Moreover, it can be concluded that the process using TiO₂-supported biochar as photocatalyst offered a better energy efficiency 136.49 kWh/m³ compared to TiO₂ which has a corresponding EE_o of 1182.19 kWh/m³. The lower EE_o does provide a cost benefit.

Table 5.2: Electrical Energy Efficiency per order (EE_o) and Kinetic parameters of orange II sodium using the TiO_2 and TiO_2 -supported biochar composites at pH 4, 6.8, 8, and 10. [C_{dye}= 20 ppm, C_{cat}= 200 mg/L, time= 120 min, power= 160W].

Photocatalyst	pH	Removal (%)	$K \times 10^{-3}$ (min^{-1})	r^2	EE_o (kWh/m^3)
TiO₂	4	20.75	1.94	0.7170	1056.75
	6.8	18.77	1.73	0.7719	1182.19
	8	16.32	1.49	0.8766	1379.36
	10	12.96	1.16	0.8273	1770.58
TiO₂-supported biochar	4	81.73	14.17	0.9549	144.57
	6.8	83.48	15.01	0.9525	136.49
	8	77.81	12.53	0.9677	163.39
	10	70.03	10.94	0.9435	187.22

5.2.6. Photocatalyst reusability

The photocatalyst was assessed for its reusability by subjecting it to three consecutive photodegradation studies. The achieved photodegradation efficiencies for the first, second and third run were 83.1 %, 82.6 %, 81.8 % respectively (Figure 5.10). A small decrease was observed after each run probably due to the loss of some active sites because of the orange II sodium dye molecules agglomerated on the photocatalyst surface. Similar results were also reported by Nguyen *et al.* (2020) after four runs indicating the high chemical and operating stabilities of the photocatalyst.

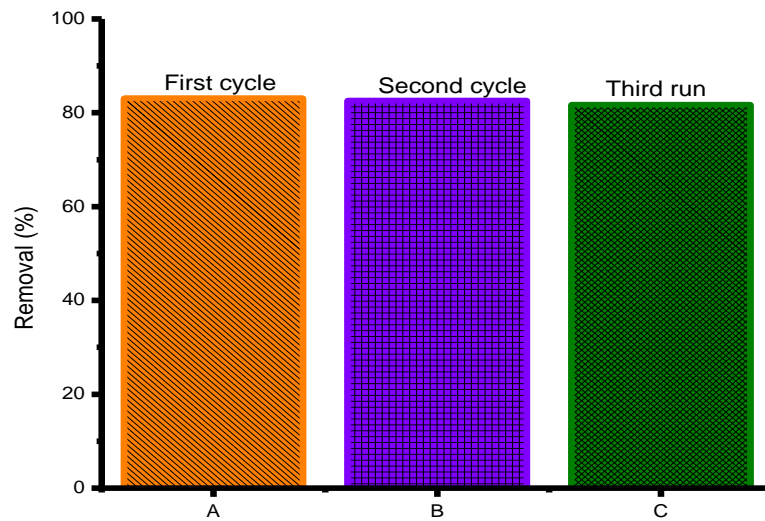


Figure 5.10: Reusability of TiO₂-supported biochar composites for orange II sodium dye for three successive cycles [C_{cat}= 200 mg/L, C_{dye}=20 ppm, time=120 min., pH= 6.8, power= 160W]

CHAPTER 6

CONCLUSIONS AND RECOMMENDATIONS

6.1. CONCLUSION

In this research, the preparation and characterization of biochar from PJW leaves, TiO₂ nanocomposite from TiCl₃, and TiO₂-supported biochar composites from mixing biochar and TiO₂ composite were successful. The optical absorption with UV-Visible spectrophotometry shows that doping TiO₂ with the biochar produce a nanocomposite with a higher response under the visible spectrum. The analysis of the morphology and amorphous structure with scanning electron microscopy (SEM) also shows that both TiO₂ and biochar are present in the composite. The chemical characterization with FTIR and the structural properties with XRD confirmed that TiO₂-supported biochar composites was successfully synthesised. The BET results show that the composite synthesised was a mesoporous material with low porosity.

The effects of different parameters such as pH, catalysts loading, and initial dye concentration were investigated on the photodegradation efficiency of orange II sodium dye using the synthesised TiO₂ and TiO₂-supported biochar composites. The optimum conditions obtained were at 120 min contact time for both composites using 200 mg/L for TiO₂ at pH 4 and TiO₂-supported biochar at pH 6.8, respectively for the degradation of 20 ppm dye. The photodegradation efficiency was found to be 18.40 % for the former and 83.48 % for the latter species respectively. The rate of degradation decreased as the initial dye concentration increased and follow the pseudo-first-order model. The neutral pH of the solution has the highest rate of reaction with the lower EE_o . Further increasing the pH (in the basic medium) and decreasing the pH (in the acidic medium) reduced the rate of the reaction with a higher EE_o . The optimum EE_o was found to be 136.49 kWh/m³ for the doped and 1056.75 kWh/m³ for the undoped nanoparticles. The photocatalyst was shown to be show negligible degradation after three consecutive photodegradation processes.

6.2. RECOMMENDATIONS

The following could be considered for future studies:

- Modification of TiO₂-supported biochar for increasing the surface area of which could increase its photo-activity.
- Application of the TiO₂-supported biochar for the treatment of raw textile wastewater.

REFERENCES

- Ahmed, M., Idris, A. & Adam, A. 2007. Removal of colour and organic pollutants from textile wastewater using integrated biological and advanced oxidation process. *J. Eng. Sci. Technol.*, 2(1): 55.
- Ajmal, A., Majeed, I., Malik, R., Idriss, H. & Nadeem, M. 2014. Principles and mechanisms of photocatalytic dye degradation on TiO₂ based photocatalysts: a comparative overview. *RSC Adv.*, 4(70): 37003-37026.
- Akpan, U.G. & Hameed, B.H. 2009. Parameters affecting the photocatalytic degradation of dyes using TiO₂-based photocatalysts: A review. *Journal of Hazardous Materials*, 170(2-3): 520-529.
- Al-Amin, M., Dey, S.C., Rashid, T.U., Ashaduzzaman, M. & Shamsuddin, S.M. 2016. Solar Assisted Photocatalytic Degradation of Reactive Azo Dyes in Presence of Anatase Titanium Dioxide. *International Journal of Latest Research. Engineering and Technology*, 2(3): 14–21.
- Al-Wabel, M.I., Al-Omran, A., El-Naggar, A.H., Nadeem, M. & Usman, A.R.A. 2013. Pyrolysis temperature induced changes in characteristics and chemical composition of biochar produced from conocarpus wastes. *Bioresource Technology*, 113: 374-379.
- Ambroz, F., Macdonald, T.J., Martis, V. & Parkin, I.P. 2018. Evolution of the BET theory for the Characterization of Meso and Microporous MOFs. *Small Methods*, 2(11): 1800173.
- Anjum, N.A., Gill, S.S. & Tuteja, N. 2017. Enhancing cleanup of environmental pollutants. *Enhancing Cleanup of Environmental Pollutants*, 2(4): 1–374.
- Au-pree, S., Narakaew, P., Thungprasert, S., Promanan, T., Chaisena, A. & Narakaew, S. 2021. Visible Light Irradiation : A Comparison of corn starch, honey, and polyethylene glycol as a carbon source. *Engineering Journal*, 25(1): 8125-8281.
- Ayoub, H., Kassir, M., Raad, M., Bazzi, H. & Hijazi, A. 2017. Effect of Dye Structure on the Photodegradation Kinetic Using TiO₂ Nanoparticles. *Journal of Materials Science and Chemical Engineering*, 5(6): 31-45.

- Badmus, K.O., Irakoze, N., Adeniyi, O.R. & Petrik, L. 2020. Synergistic advance Fenton oxidation and hydrodynamic cavitation treatment of persistent organic dyes in textile wastewater. *Journal of Environmental Chemical Engineering*, 8: 2.
- Badmus, K.O., Wewers, F., Al-Abri, M., Shahbaaz, M. & Petrik, L.F. 2021. Synthesis of oxygen deficient TiO₂ for improved photocatalytic efficiency in solar radiation. *Catalysts*, 11(8): 1–15.
- Batista, R.R. & Gomes, M.M. 2021. Effects of chemical composition and pyrolysis process variables on Biochar yields: correlation and principal component analysis. *Forest Products Science and Tecnology, Floresta e Ambiente*, 28(3): 2-12.
- Beydoun, D. & Amal, R. 2002. Implications of heat treatment on the properties of a magnetic iron oxide-titanium dioxide photocatalyst. *Materials Science and Engineering B*, 94(1): 71–81.
- Berthomieu, C. & Hienerwadel, R. 2009. Fourier transform infrared (FTIR) spectroscopy. *Photosynthesis Research*, 101(2-3): 157-170.
- Bolton, J., Bircher, K., Tumas, W. & Tolman, C. 2001. Figures-of-merit for the technical development and application of advanced oxidation technologies for both electric- and solar-driven systems (IUPAC Technical Report). *Pure and Applied Chemistry*, 73(4): 627-637.
- Brown, M.A. & DeVito, S.C. 1993. Predicting azo dyes toxicity. *Crit. Rev. Environ. Sci. Technolo*, 23: 249-324.
- Bunaciu, A.A., Udriștioiu, E.G. & Aboul-Enein, H.A. 2015. X-Ray Diffraction: Instrumentation and Applications, *Critical Reviews in Analytical Chemistry*, 45(4): 289-299.
- Castro, A.M., Lopes, I. & Rocha-santos, T. 2019. applied sciences Evaluation of the Potential Toxicity of Effluents from the Textile Industry before and after Treatment. *Appl. Sci.*, 9(18): 384.
- Chandran, D. 2015. A Review of the Textile Industries Waste Water Treatment Methodologies. *International Journal of Scientific & Engineering Research*, 7(1): 392–403.
- Chao, C., Mingce, L., Hui, Z., Weimin, C., Baoxue, Z., Jingyi, Z., Yahui, W., Dawei, D. & Deyong, W. 2009. Preparation, characterization and visible-light activity of carbon modified TiO₂ with two kinds of carbonaceous species. *Journal of Molecular Catalysts A: Chemical*,

314(1-2): 35-41.

Cheol, H.K., Ui-Su, I., Sang, W.S., Kim, M.II, Yun, S.H. & Ji, S.I. 2021. Effects of carbon doping on TiO₂ for enhanced visible light-driven NO sensing performance. *Materials Letters*, 288: 129313.

Chiu, Y.H., Chang, T.F.M., Chen, C.Y., Sone, M. & Hsu, Y.J. 2019. Mechanistic insights into photodegradation of organic dyes using heterostructure photocatalysts. *Catalysts*, 9(5):430.

Chong, M.; Jin, B.; Chow, C. & Saint, C. 2010. Recent developments in photocatalytic water treatment technology: A review. *Water Research*, 44(10): 2997-3027.

Choudhury, A.K.R. 2018. Eco-friendly dyes and dyeing. *Advanced Materials and Technologies for Environmental Applications*, 2(1): 145-176.

Cloete, T.E., Kwaadsteniet, M.D., Botes, M. & Lopez-Romero, J.M. 2010. Nanotechnology in Water Treatment Applications. *Caister Academic Press*, 196.

Cronk, Q.C.B. & Fuller, J.L. 1995. Plant invaders: the treat to natural ecosystems. *Chapman & Hall Ltd*, 241.

de Oliveira, P.L., Marques, S.I., Pereira, Z.L., Silveira, V.S., Do Rosário, G.I. & Magalhães, F. 2019. Preparation of magnetic photocatalysts from TiO₂, activated carbon and iron nitrate for environmental remediation. *Journal of Photochemistry and Photobiology A: Chemistry*, 382(3): 111907.

Donga, S., Fenga, J., Fanc, M., Pia, Y., Hua, L., Hana, X., Liua, M., Sunb, J. & Suna, J. 2015. Recent developments in heterogeneous photocatalytic water treatment using visible-light-responsive photocatalysts: A review. *RSC Adv.*, 5: 14610-14630.

Eletta, O.A.A., Mustapha, S.I., Ajayi, O.A. & Ahmed, A.T. 2018. Optimization of dye removal from textile wastewater using activated carbon from sawdust. *Nigerian Journal of Technological Development*, 15(1): 26.

Enqvist, J.P. & Ziervogel, G. 2019. Water governance and justice in Cape Town: An overview. *Wiley Interdisciplinary Reviews: Water*, 4: 1354.

Ezzatahmadi, N., Bao, T., Liu, H., Graeme, J., Millar, Ayoko, G.A., Zhu, J., Zhu, R. Liang, X., Hee, H. & Xi, Y. 2018. Catalytic degradation of Orange II in aqueous solution using

diatomite-supported bimetallic Fe/Ni nanoparticles. *RSC Advances*, 8 : 7687-7696.

- Fluence News Team 2019. Textile Industry Water Use and Treatment, February. <http://www.fluencecorps.com/textile-industry-water-use/> [Accessed: 12 July 2019].
- French, R.W. 2009. Extinction coefficient of Dyes. *Stain Technology*, 2(4): 124-125.
- Fu, G.Y. & Viraghavan, T. 2001. Fungal decolorization of Dyes wastewater -A review. *Bioresource Technology*, 79(3): 51-62.
- Gautam, R.K. & Chattopadhyaya, M.C. 2017. Nanomaterials for wastewater Remediation. *MRS Bulletin*, 42(9): 685-686.
- Garrido-Cardenas, J.A., Esteban-García; B., Agüera; A., Sánchez-Pérez, J.A. & Manzano-Agugliaro, F. 2020. Wastewater treatment by advanced oxidation process and their worldwide research trends. *International Journal of Environmental Research and Public Health*, 17: 170-188.
- Gee, E.L. , Che Azurahaman Che Abdullah, Wan Amir Nizam Wan Ahmad Suvik Assaw & Alvin Lim Teik Zheng 2020. Eco-Friendly Photocatalysts for Degradation of Dyes. *Catalysts*, 10: 1129.
- Ghaly, A.E., Ananthashankar, R., Alhattab, M. & Ramakrishnan, V.V. 2013. Production, Characterization and Treatment of Textile Effluents: A Critical Review. *Journal of Chemical Engineering & Process Technology*, 05(01): 1–19.
- Ghasemia, S., Rahimnejada, S., Rahman, S., Setayesha, S., Rohanib, S. & Gholami, M.R. 2009. Transition metal ions effect on the properties and photocatalytic activity of nanocrystalline TiO₂ prepared in an ionic liquid . *Journal of Hazardous Materials*, 172 (2–3): 1573-1578.
- Gnanaprakasam, A., Duraibabu, D. & Kumar, S.A. 2015. Synthesis and Characterization of Ether Containing Tetraglycidyl Epoxy Reinforced with Amine Functionalized Graphene Oxide (F-Go) and It's Nanocomposites . *Journal of Polymer & Composites*, 3(2): 39-51.
- Greer, A.L., Keane, S.E. & Lin, Z. 2010. NRDC's Ten Best Practices for Textile Mills to Save Money and Reduce Pollution. *NRDC Clean By Design*, 2.
- Gong, Q. & Hart, B.A. 1997. Effect of Thiols on Cadmium-Induced Expression of Metallothionein and Other Oxidant Stress Genes in Rat Lung Epithelial Cells. *Toxicology*, 119, 179-191.

- Gorska, P., Zaleska, A., Kowalska, E., Klimczuk, T., Sobczak, J.W., Swarek, E., Janusz, W., Hupka, J. 2008. TiO₂ photo-activity in vis and UV light: The influence of calcination temperature and surface properties. *Applied Catalysis B: Environmental*, 84 (3-4): 440-447.
- Guo, J., Kang, L., Wang, X. & Jingliang Y. 2010. Decolorization and Degradation of Azo Dyes by Redox Mediator System with Bacteria. *Biodegradation of Azo Dyes, Hdb Env Chem*, 9: 85–100.
- Haroun, M, Idris, A. and Omar, S. 2009. Analysis of heavy metal during Compositing of the Tannery Sludge Using Physicochemical and Spectroscopic Techniques. *Journal of Hazardous Materials*, 65: 111-119.
- Hassaan, M.A. 2016. Advanced oxidation processes of some organic pollutants in fresh and seawater (PhD thesis). Faculty of Science, Port Said University.
- Hassaan, M.A. & Nemr, A.E. 2017. Environment and Sustainability Health and Environmental Impacts of Dyes : Mini Review. *Environment and Sustainability*, 1(13): 64–67.
- Hassaan, M.A. & Ahmed, E.N. 2017. Health and Environmental Impacts of Dyes: Mini Review. *Engineering*, 1(3): 64-67.
- Hildegard, D.B. 1987. Port Jackson Willow. *Farming in South Africa*, 8.
- Hu, S.Z., Li, F.Y., Fan, Z.P. & Zhang, J. 2013. An improved calcination route to synthesize carbon doped mesoporous TiO₂ and its photocatalytic activity under visible light. *Asian Journal of Chemistry*, 25(16): 9199-9202.
- Huang, D.Y., Zhou, S.G., Ghen, Q., Zhao, B., Yuan, Y., & Zhuang, L. 2011. Enhanced anaerobic degradation of organic pollutants in a soil microbial fuel cell. *Chemical Engineering Journal*, 172: 647-653.
- Hoffmann, M.R., Martin, S.T., Choi W. & D.W. 1995. Bahnemann, Environmental applications of semiconductor photocatalysis. *Chemical Reviews*, 95(1): 69–96.
- Irani, M., Mohammadi, T. & Mohebbi, S. 2016. Photocatalytic Degradation of Methylene Blue with ZnO Nanoparticles; a Joint Experimental and Theoretical Study. *Journal of the Mexican Chemical Society*, 60(4): 218-225.
- Jadaa, W., Prakash, A. & Ray, A.K. 2021. Photocatalytic Degradation of Diazo Dye over

- Suspended and Immobilized TiO₂ Catalyst in Swirl Flow Reactor: Kinetic Modeling. *Processes*, 9, 1741.
- Jamil, T.S., Ghaly, M.Y., Fathy, N.A., Abd el-halim, T.A., Österlund L. 2012. Enhancement of TiO₂ behavior on photocatalytic oxidation of MO dye using TiO₂/AC under visible irradiation and sunlight radiation. *Separation and Purification Technology*, 98: 270–279.
- Jensen, H., Pedersen, J.H., Jørgensen, J.E., Pedersen, J.S., Joensen, K.D., Iversen, S.B. & Søggaard, E.G. 2006. Determination of size distributions in nanosized powders by TEM, XRD, and SAXS. *Journal of Experimental Nanoscience*, 1(3): 355–373.
- Joni, I.M., Nulhakim, L. & Panatarani, C. 2018. Characteristics of TiO₂ particles prepared by simple solution method using TiCl₃ precursor. *Journal of Physics: Conf. Series*, 1080: 012042.
- Kanakaraju, D., Glass, B.D. & Oelgemoeller, M. 2014. *Environ. Chem. Lett.*, (12): 27-47.
- Kang, X., Liu, S., Dai, Z., He, Y., Song, X. & Tan, Z. 2019. Titanium dioxide: From engineering to applications. *Catalysts*. 9(2): 191.
- Khan, R. & Banerjee, U.C. 2010. Decolorization of Azo Dyes by Immobilized Bacteria. *Biodegradation of Azo Dyes, Hdb Env Chem.*, 9: 73-84.
- Ki-Hyun, Kim, Jahan, S.A., Kabir, E. & Brown, R.J.C. 2013. A Review of Airborne Polycyclic Aromatic Hydrocarbons (PAHs) and Their Human Health Effects. *Environ*, 60: 71-80.
- Klaysri, R., Ratova, M., Prasertdam, P. & Kelly, P. 2017. Deposition of visible light active C-doped Titania films via magnetron sputtering using CO₂ as a source of carbon. *Nanomaterials*, 7(5): 113.
- Kumar, A. 2016. Environmental Pollution by Textile Industries. *Anthropogenic Pollution : Causes and Concern*, 1–8.
- Kumar, A. 2018. Different Methods Used for the Synthesis of TiO₂ Based Nanomaterials: A Review. *American Journal of Nano Research and Applications*, 6(1): 1.
- Kursvuran, E., Irmak, S., Yavuz H.I., Samile A. & Erbatur O. 2005. Comparison of the treatment methods efficiency for the decolorization and mineralization of Reactive Black 5 azo dye. *J. Hazard. Mater.*, 119: 109-116.

- Kuzyakov, Y., Subbotina, I., Chen, H., Bogomolova, I. & Xu, X. 2009. Black carbon decomposition and incorporation into soil microbial biomass estimated by ^{14}C labeling. *Soil Biology and Biochemistry*, 41(2): 210–219.
- Laxman M.S. 2009. Pollution and its Control in Textile Industry. *Dyes and Chemicals*.
[//www.fibre2fashion.com/industry-article/4434/pollution-and-its-control-intextile-industry](http://www.fibre2fashion.com/industry-article/4434/pollution-and-its-control-intextile-industry). [Accessed: 04 March 2021].
- Lee, S. & Park, S. 2013. TiO_2 photocatalyst for water treatment applications. *Journal of Industrial and Engineering Chemistry*, 19(6): 1761-1769.
- Lellis, B., Fávaro-Polonio, C.Z., Pamphile, J.A. & Polonio, J.C. 2019. Effects of textile dyes on health and the environment and bioremediation potential of living organisms. *Biotechnology Research and Innovation*, 3(2): 275–290.
- Li, Y.J., Yang, C., Guo, X.T., Dang, Z., Li, X.Q., Zhang, Q. 2015. Effects of humic acids on the aggregation and sorption of nano- TiO_2 . *Chemosphere*, 119: 171-176.
- Lin, L., Chai, Y., Zhao, B., Wei, W., He, D., He, B. & Tang, Q. 2013. Photocatalytic oxidation for degradation of VOCs. *Open Journal of Inorganic Chemistry*, 3: 14-25.
- Liu, J., Gao, Z.Y., Chen, K.Y. Song, C.X., Wang, D.Q. & He, Y.L. 2019. Photocatalytic Degradation of Dye Wastewater by NG/ TiO_2 Composite. International Conference on Power, Energy. *Environment and Material Science*, (PEEMS 2019).
- Madhusudhana, N, Yogendra, K. & Mahadevan, K.M. 2012. A comparative study on Photocatalytic degradation of Violet GL2B azo dye using CaO and TiO_2 nanoparticles. *International Journal of Engineering Research and Applications*, 2(5): 1300-1307.
- Mahlambi, M.M., Ngila, C.J. & Mamba, B.B. 2015. Recent developments in environmental photocatalytic degradation of organic pollutants: The case of titanium dioxide nanoparticles- A review. *Journal of Nanomaterials*. 2015: 29.
- Mainya, N.O., Tum, P. & Muthoka, T.M. 2013. Photodegradation and Adsorption of Methyl Orange and Methylene Blue Dyes on TiO_2 . *Int. J. Sci. Res.*, 4: 3185-3189.
- Makula, P., Pacia, M. & Macyk, W. 2018. How To Correctly Determine the Band Gap Energy of Modified Semiconductor Photocatalysts Based on UV–Vis Spectra. *J. Phys. Chem. Lett.* 9(23): 6814–681.

- Maulidiyah, D.W., Hikmawati, R.S. & Nurdin, M. 2015. Preparation and Characterization of Activated Carbon from Coconut Shell - Doped TiO₂ in Water Medium. *Oriental Journal of Chemistry*, 31(4): 2337-2342.
- McMullan, G.A., Conneely, C.M. & Kirby, N. 2001. Microbial decolourisation and degradation of textiles dyes. *Applied Microbiology and Biotechnology*, 55(1-2): 81 -87.
- Mian, M.M. & Liu, G. 2018. Recent progress in biochar-supported photocatalysts: Synthesis, role of biochar, and applications. *RSC Advances*, 8(26): 14237–14248.
- Midgley, S.J. & Turnbull, J.W. 2003. Domestication and use of Australian acacias: Case studies of five important species. *Australian Systematic Botanic*, 16 (1): 89-102.
- Mota, A.L.N., Albuquerque, L.F., Beltrame, L.T.C., Chiavone-Filho, O., Machulek, J.A. & Nascimento, C.A.O. 2008. Advanced oxidation processes and their application in the petroleum industry: A Review. *Brazilian Journal of Petroleum and Gas*, 2(3): 122-142.
- Muhich, C.L., Westcott, J.Y., Fuerst, T., Weimer, A.W. & Musgrave, C.B. 2014. Increasing the photocatalytic activity of anatase TiO₂ through B, C, and N doping. *J. Phys. Chem.*, 118: 27415–27427 .
- Mondol, B., Sarker, A., Shareque, A.M., Dey, S.C., Islam, M.T., Das, A.K., Shamsuddin, S.M., Molla, M.A.I., Sarker, M. 2021. Preparation of Activated Carbon? TiO₂ Nanohybrids for Photodegradation of Reactive Red-35 Dye Using Sunlight. *Photochem*, 1: 54-66.
- Moyet, M.A. 2019. Synthesis and Characterization of Heteronuclear Inorganic Complexes for the Photodegradation of Persistent Organic Pollutants. *Electronic Theses and dissertation*, 3056.
- Neimark, A.V., Sing, K.S.W. & Thommes, M. 2008. Characterization of Solid Catalysts. *Handbook of Heterogeneous Catalysis*, 2: 721-738.
- Nielsen, S.S. 2010. Food analysis. *Food Science Texts Series*, 4: 106-115.
- Nguyen, C.H., Tran, H.N., Fu, C.C., Lu, Y.T. & Juang, R.S. 2020. Roles of adsorption and photocatalysis in removing organic pollutants from water by activated carbon–supported Titania composites: Kinetic aspects. *Journal of the Taiwan Institute of Chemical Engineers*, 109: 51–61.

- Nova, L., Nova, L., Mota, A.L.N., Albuquerque, L.F., Beltrame, L.T.C., Chiavone, F.O., Machulek Jr, A., Nascimento, C.A.O. 2009. Advanced oxidation processes and their application in the petroleum industry: a review. *Brazilian Journal of Petroleum and Gas*, 2(3): 122–142.
- Ohashi, T., Jara, A.M.T., Batista, A.C.L., Franco, L.O., Lima, M.A.B., Benachour, M., Da Silva, C.A.A. & Campos, T.G.M. 2012. An improved method for removal of azo dye orange II from textile effluent using albumin as sorbent. *Molecules*, 17(12): 14219–14229.
- Oliveira, G.A., Gevaerd, A., Mangrich, A.S., Marcolino-Junior, L.H. & Bergamini, M.F. 2021. Biochar obtained from spent coffee grounds: Evaluation of adsorption properties and its application in a voltammetric sensor for lead (II) ions. *Microchemical Journal*, 165(6): 106114.
- Onyatta, J., Tum, P., Kithure, J. & Oduor., F. 2016. Photocatalytic Degradation of Acid Orange Ii Dye on Selected Commercial Titanium Dioxide Catalysts. *International Journal of Advanced Research*, 4(10), 1149–1155.
- Ou, X.H., Wu, C.H. & Lo, S.L. 2006. Photodegradation of 4-chlorophenol by UV/photocatalysts: the effect of the interparticle electron transfer process. *Reaction Kinetics and Catalysis Letters*, 88(1): 89–95.
- Ozer, C. & Kevser, D. 2010. Biodegradation of Azo Dyes in Anaerobic–Aerobic Sequencing Batch Reactors. *Biodegradation of Azo Dyes, Hdb Env Chem.*, 9: 59–72.
- Palter, J.B., Marinov, I., Sarmiento, J.L. & Gruber, N. 2006. Large-Scale, Persistent Nutrient Fronts of the World. *Handbook of Environmental Chemistry*, 5.
- Park, II, Abiko, T. & Okabe, T.H. 2005. Production of titanium powder directly from TiO₂ in CaCl₂ by Electronically Mediated Reaction (EMR). *Journal of Physics and Chemistry of Solids*, 66(2): 410-413.
- Pelaez, M., Nolan, N.T., Pillai, S.C., Seery, M.K., Falaras, P., Kontos, A.G., Dunlop, P.S.M., Hamilton, J.W.J., Byrne, J.A., O’Shea, K., Entezari, M.H. & Dionysiou, D.D. 2012. A review on the visible light active titanium dioxide photocatalysts for environmental applications. *Applied Catalysis B: Environmental*, 125: 331–349.
- Pengelly, C., Seyler, H., Fordyce, N., Vuuren, P.JV., Walt, M.V.D., Zyl, H.V., Kinghorn, J. 2017.

- Managing water as a constraint to development with decision-support tools that promote integrated planning: The case of the Berg Water Management Area (WRC ProjectNo. K5/2453).
- Radha, E., Komaraiah, D., Reddy M.V.R., Sayanna, R., Sivakumar, J. 2018. Structural, optical and photocatalytic properties of anatase/rutile TiO₂ nanoparticles. *Journal on Material Science*, 6(3): 43-48.
- Ranga, S. 2017. Comparative Analysis of Homogeneous and Heterogeneous Catalysis. *International Journal of Engineering Technology Science and Research*, 4(9): 1496-1500.
- Rashed, M.N., Eltaher, M.A. & Abdou, A.N.A. 2017. Adsorption and photocatalysis for methyl orange and Cd removal from wastewater using TiO₂/sewage sludge-based activated carbon nanocomposites. *Royal Society Open Science*, 4: 12.
- Riaz, N. 2013. Preparation of Cu-Ni/TiO₂ photocatalyst and its application in orange ii removal under visible light irradiation (PhD). Chemical engineering department, Bandar Seriiskandar, Perak, Pakistan.
- Richardson, D.M. & Kluge, R.L. 2008. Seed banks of invasive Australian Acacia species in South Africa: Role in invasiveness and options for management. *Perspectives in plant Ecology Evolution & Systematics*, 10(3): 161-177.
- Richardson, D.M., Moran, V.C., Le Maitre, D.C., Rouget, M. & Foxcroft, L.C. 2004. Recent developments in the science and management of invasive alien plants: connecting the dots of research knowledge, and linking disciplinary boxes. *South African Journal of Science*, 100: 126-128.
- Sadaka, S., Sharara, M.A., Ashworth, A., Keyser, P., Allen, F. & Wright, A. 2014. Characterization of biochar from Switchgrass carbonization. *Energies*, 7: 548-567.
- Saggiaro, E.M., Oliveira, A.S., Pavesi, T., Maia, C.G., Ferreira, L.F.V. & Moreira, J.C. 2011. Use of titanium dioxide photocatalysis on the remediation of model textile wastewaters containing azo dyes. *Molecules*, 16(12): 10370–10386.
- Sandhya, S. 2010. Biodegradation of Azo Dyes Under Anaerobic Condition: Role of Azoreductase. *Hdb Env Chem.*, 9: 39–57.
- Saraswati, T.E. , Andhika, I.F., Nandika, A.O., Wahuningsih, S. & Purnawana, C. 2015.

Synthesis And Surface Modification Of TiO₂/Carbon Photocatalyst Produced By Arc Discharge In Ethanol Medium. *Material Chemistry*, 1: 110-113.

Sarunas Varnagirisa, Arturs Medvid ,Martynas Lelisa ,Darius Milcius & Andris Antuzevic 2019. Black carbon-doped TiO₂ films: Synthesis, characterization and photocatalysis. *Journal of Photochemistry and Photobiology A: Chemistry*, 382: 111941.

Semeraro, P., Rizzi, V., Fini, P., Matera, S., Cosma, P., Franco, E., Garcia, R., ferrandiz, M., Nunez, E., Gabaldon, A., Fortea. I., Perez, E. & Ferrandiz, M. 2015. Interaction between industrial textile dyes and cyclodextrins. *Dyes and Pigments*, 119: 84-94.

Shyan, P., Karthikeyan, S.N. & Prablu, K.H. 2007. Wastewater and its treatment in textile industry (PhD), Department of Fibres and Textiles Processing Technology. 40019.

Singh, P., Vishnu, M.C., Sharma, K.K., Singh, R., Madhav, S., Tiwary, D. & Mishra, P.K. 2016. Comparative study of dye degradation using TiO₂-activated carbon nanocomposites as catalysts in photocatalytic, sonocatalytic, and photosonocatalytic reactor. *Desalination and Water Treatment*, 57(43): 20552–20564.

Sintayehu, Y.D., Gemeta, A.B., Berehe S.G. 2017. Optical Photocatalytic Degradation of Methylene Blue Using Lignocellulose Modified TiO₂. *American Journal of Optics and Photonics*, 5(5): 55-58.

Stasinakis, A.S. 2008. Use of selected advanced oxidation processes (AOPs) for wastewater treatment - A mini review. *Global Nest Journal*, 10(3): 376–385.

Stella, M.G., Sugumaran, P., Niveditha, S., Ramalakshmi, B., Ravichandran, P. & Seshadri, S. 2016. Production characterization and evaluation of biochar from Pod (Pisum Sativum), Leaf (Brassica Oleracea), and Peel (Citrus Sinensis) wastes. *International Journal of Recycling of Organic Waste in Agriculture*, 5: 43-53.

Stewart, B.D. 2018. Photocatalysis using TiO₂ nanoparticles containing surface metal sites. Master's theses and capstones. New Hampshire, Durham, 1222.

Studies, A. 2011. Advanced Oxidation Processes (AOPs) applied for wastewater and drinking water treatment . *Elimination of Pharmaceuticals*, 1: 63–74.

Subramani, A.K., Byrappa, K., Ananda, S., Lokanatha R.K.M., Ranganathaiah, C., & Yoshimura, M. 2007. Photocatalytic degradation of indigo carmine dye using TiO₂ impregnated

- activated carbon. *Bulletin of materials science*, 30(1): 37-41.
- Spokas, K.A., Cantrell, K.B., Novak, J.M., Archer, D.W., Ippolito, J.A., Collins, H.P., Boateng, A.A., Lima, I.M., Lamb, M.C., McAloon, A.J., Lentz, R.D. & Nichols, K.A. 2012. Biochar: A Synthesis of Its Agronomic Impact beyond Carbon Sequestration. *Journal of Environmental Quality*, 41(4): 973-989.
- Syafei, D., Sugiarti, S., Darmawam N. & Khotib, M. 2017. Synthesis of TiO₂/ carbon nanoparticle (C-dot) composites as active catalysts for photodegradation of persistent organic pollutant. *Indones. J. Chem.*, 17(1): 37-42.
- Varnagiris, S., Medvids, A., Lelis, M., Milcius, D. & Antuzevics, A. 2019. Black carbon-doped TiO₂ films: Synthesis, characterization and photocatalysis. *Journal of Photochemistry and Photobiology A: Chemistry*, 382: 111941.
- Vineta, S., Silvana, Z., Sanja, R. & Golomeova, S. 2014. Methods for wastewaters treatment in textile industry. *In International Scientific Conference, Gabrovo*, 248-252.
- Wang, Z.; Xue, M.; Huang, K. & Liu, Z. (2011). Textile dyeing wastewater treatment. *Treating Textile Effluent*, 91–116.
- WHO. Air quality guidelines for Europe (2000). 2nd edition.
- WHO. The world health report (2002) - Reducing Risks, Promoting Healthy Life.
- Wei, M., Feng, W., Dong, X., Yongxiang, L. & Zhonglin, M. 2014. Structure and composition study of carbon-doped titanium oxide film combined with first principles. *Journal of Advanced ceramics*, 3(1): 49-55.
- Wei, S.-W., Peng, B., Chai, L.-Y., Liu, Y.-C. & Li, Z.-Y. 2008. Preparation of doping titania antibacterial powder by ultrasonic spray pyrolysis, *Transactions of Nonferrous Metals. Society of China*, 18(5): 1145–1150.
- Xing, B., Shi, C., Zhang, C., Yi, G., Chen, L., Guo, H., Huang, G. & Cao, J. 2016. Preparation of TiO₂/Activated Carbon Composites for Photocatalytic Degradation of RhB under UV Light Irradiation. *Journal of Nanomaterials*, 2016: Article ID 8393648.
- Yang, H., Yan, R., Chin, T., Liang, D.T., Chen, H. & Zheng, C. 2004. Thermogravimetric Analysis-Fourier Transform Infrared Analysis of Palm Oil Waste Pyrolysis, *Energy &*

Fuels, 18: 1814-1821.

- Yang, M., Han-Qing, Y., Jia-Chuan, Z. & Shu-Juan, Z. 2004. TiO₂-mediated photocatalytic degradation of Orange II with the presence of Mn²⁺ in solution. *Journal of Photochemistry and Photobiology A: Chemistry*, 163: 311–316.
- Yetim, T. & Tekin, T. 2016. A Kinetic Study on Photocatalytic and Sonophotocatalytic Degradation of Textile Dyes, *Periodica Polytechnica Chemical Engineering*, 8535.
- Zhang, D., Li, G., Wang, F. & Yu, J.C. 2010. Green synthesis of a self-assembled rutile mesocrystalline photocatalyst. *The Royal Society of Chemistry Cryst. Eng. Com.*, 12: 1759-1763.
- Zhang, J.; Liu, F.; Gao, J.; Chen, Y. & Hao, X. 2017. Ordered Mesoporous TiO₂/Activated Carbon for Adsorption and Photocatalysis of Acid Red 18 Solution. *BioResources*, 12(4): 9086–9102.
- Zhang, M., Gao, B., Yao, Y., Xue, Y. & Inyang, M. 2012. Synthesis, characterization, and environmental implications of graphene-coated Biochar. *Science of the Total Environment*, 567–572.
- Zhang, N., Liu, S., Fu, X. & Xu, Y.J. 2011. Synthesis of M-TiO₂ (M = Au, Pd, Pt) Core-Shell Nanocomposites with Tunable Photoreactivity. *Journal of Physical Chemistry C.*, 15: 9136–9145.
- Ziervogel, G. & Parnell, S. 2014. Tackling barriers to climate change adaptation in South African coastal cities. *The Netherlands: Springer Science + Business Media*. 57–73.